The Vertical City Weather Generator (VCWG v1.3.0)

Mohsen Moradi[1], Benjamin Dyer[1], Amir Nazem[1], Manoj K. Nambiar[1], M. Rafsan Nahian[1],
Bruno Bueno[4], Chris Mackey[6], Saeran Vasanthakumar[7], Negin Nazarian[2], E. Scott Krayenhoff[3], Leslie
K. Norford[5], and Amir A. Aliabadi[1]

[1]School of Engineering, University of Guelph, Guelph, Canada
[2]Built Environment, University of New South Wales, Sydney, Australia
[3]School of Environmental Sciences, University of Guelph, Guelph, Canada
[4]Fraunhofer Institute for Solar Energy Systems ISE, Freiburg, Germany
[5]Department of Architecture, Massachusetts Institute of Technology, Cambridge, USA
[6]Ladybug Tools LLC, Boston, USA
[7]Kieran Timberlake Research Group, Philadelphia, USA

Correspondence: Amir A. Aliabadi (aliabadi@uoguelph.ca)

Abstract. The Vertical City Weather Generator (VCWG) is a computationally efficient urban micro-climate model developed
to predict temporal and vertical variation of potential temperature, wind speed, specific humidity, and turbulence kinetic energy.
It is composed of various sub-models: a rural model, an urban vertical diffusion model, a radiation model, and a building energy
model. Forced with weather data from a nearby rural site, the rural model is used to solve for the vertical profiles of potential
temperature, specific humidity, and friction velocity at 10 m above ground level (a.g.l.). The rural model also calculates a
horizontal pressure gradient. The rural model outputs are applied to a vertical diffusion urban micro-climate model that solves
vertical transport equations for temperature, momentum, specific humidity, and turbulence kinetic energy. The urban vertical
diffusion model is also coupled to the radiation and building energy models using two-way interaction. The aerodynamic
and thermal effects of urban elements, surface vegetation, and trees are considered. The predictions of the VCWG model
are compared to observations of the Basel UrBan Boundary Layer Experiment (BUBBLE) micro-climate field campaign for
eight months from December 2001 to July 2002. The model evaluation indicates that the VCWG predicts vertical profiles of
meteorological variables in reasonable agreement with the field measurements. The average BIAS, RMSE, and R^2 for potential
temperature are 0.25 K, 1.41 K, and 0.82, respectively. The average BIAS, RMSE, and R^2 for wind speed are 0.67 $\mathrm{ms^{-1}}$, 1.06
$\mathrm{ms^{-1}}$, and 0.41, respectively. The average BIAS, RMSE, and R^2 for specific humidity are 0.00057 $\mathrm{kgkg^{-1}}$, 0.0010 $\mathrm{kgkg^{-1}}$,
and 0.85, respectively. In addition, the average BIAS, RMSE, and R^2 for Urban Heat Island (UHI) are 0.36 K, 1.2 K, and
0.35, respectively. Based on the evaluation, the model performance is comparable to the performance of similar models. The
performance of the model is further explored to investigate the effects of urban configurations such as plan and frontal area
densities, varying levels of vegetation, building energy configuration, radiation configuration, seasonal variations, and different
climate zones on the model predictions. The results obtained from the explorations are reasonably consistent with previous
studies in the literature, justifying the reliability and computational efficiency of VCWG for operational urban development
projects.

1 Introduction

Urban areas interact with the atmosphere through various exchange processes of heat, momentum, and mass, which substantially impact human comfort, air quality, and energy consumption. Such complex interactions are observable from the Urban Canopy Layer (UCL) to a few hundred meters within the Atmospheric Boundary Layer (ABL) (Britter and Hanna, 2003). Modeling enables a deeper understanding of interactions between urban areas and the atmosphere and can possibly offer solutions toward mitigating adverse effects of urban development on the climate. A brief review of modeling efforts is essential toward more accurate model development for the understanding of urban areas-atmosphere interactions.

Meso-scale models incorporating the urban climate were initially aimed to resolve weather features with grid resolutions of at best a few hundred meters horizontally and a few meters vertically, without the functionality to resolve micro-scale three-dimensional flows or to account for atmospheric interactions with specific urban elements such as roads, roofs, and walls (Bornstein, 1975). These models usually consider the effect of built-up areas by introducing an urban aerodynamic roughness length (Grimmond and Oke, 1999) or adding source or sink terms in the momentum (e.g. drag term) and temperature (e.g. anthropogenic heat term) equations (Dupont et al., 2004). Therefore, if higher grid resolutions less than ten meters (horizontal and vertical) are desired (Moeng et al., 2007; Wang et al., 2009; Talbot et al., 2012), micro-scale climate models should be deployed. ~~Some efforts have also begun by investigators to develop~~ Recently, multi-scale climate models ~~by coupling have coupled~~ meso-scale and micro-scale models (Chen et al., 2011; Kochanski et al., 2015; Mauree et al., 2018). Numerous studies have used Computational Fluid Dynamics (CFD) to investigate the urban micro-climate taking into account interactions between the atmosphere and the urban elements with full three-dimensional flow analysis (Saneinejad et al., 2012; Blocken, 2015; Nazarian and Kleissl, 2016; Aliabadi et al., 2017; Nazarian et al., 2018). Despite accurate predictions, CFD models are not computationally efficient, particularly for weather forecasting at larger scales and for a long period of time, and they usually do not represent many processes in the real atmosphere such as clouds and precipitation. As an alternative, Urban Canopy Models (UCMs) require understanding of the interactions between the atmosphere and urban elements to parameterize various exchange processes of radiation, momentum, heat, and moisture within and just above the canopy, based on experimental data, physical processes from theoretical considerations, three-dimensional simulations, or simplified urban configurations (Masson, 2000; Kusaka et al., 2001; Martilli et al., 2002; Chin et al., 2005; Krayenhoff et al., 2014, 2015; Nazarian and Kleissl, 2016; Aliabadi et al., 2019). These urban canopy models are more computationally efficient than CFD models. They are designed to provide more details on heat storage and radiation exchange, while they employ less detailed flow calculations.

Urban micro-climate models must account for a few unique features of the urban environment. Urban obstacles such as trees and buildings contribute substantially to the changing of flow and turbulence patterns in cities (Kastner-Klein et al., 2004). Difficulties arise when the spatially inhomogeneous urban areas create highly three-dimensional wind patterns that result in the difficulty of parameterizations (Roth, 2000; Resler et al., 2017). For example, the surfaces of urban obstacles exert form and skin drag and consequently alter flow direction and produce eddies at different spatio-temporal scales. This can lead to the formation of shear layers at roof level with variable oscillation frequencies (Tseng et al., 2006; Masson et al., 2008; Zajic et al., 2011), all of such phenomena should be properly approximated in parameterizations.

Heat exchanges between the indoor and outdoor environments significantly influence the urban micro-climate. Various studies have attempted to parametrize heat sources and sinks caused by buildings such as heat fluxes due to infiltration, exfiltration, ventilation, walls, roofs, roads, windows, and building energy systems (e.g. condensers and exhaust stacks) (Kikegawa et al., 2003; Salamanca et al., 2010; Yaghoobian and Kleissl, 2012). Therefore, a Building Energy Model (BEM) is required to be properly integrated in an urban micro-climate model to take account of the impact of building energy performance on the urban micro-climate (Bueno et al., 2011, 2012b; Gros et al., 2014). This two-way interaction between the urban micro-climate and indoor environment can significantly affect Urban Heat Island (UHI) [K] and energy consumption of buildings (Salamanca et al., 2014).

Urban vegetation can substantially reduce the adverse effects of UHI [K], particularly during heat waves, resulting in improved thermal comfort (Grimmond et al., 1996; Akbari et al., 2001; Armson et al., 2012). Urban trees can potentially provide shade and shelter, and therefore, change the energy balance of the individual buildings as well as the entire city (Akbari et al., 2001). A study of the local-scale surface energy balance revealed that the amount of energy dissipated due to the cooling effect of trees is not negligible and should be parameterized properly (Grimmond et al., 1996). In addition, the interaction between urban elements, most importantly trees and buildings, is evident in radiation trapping within the canyon and shading impact of trees (Krayenhoff et al., 2014; Redon et al., 2017; Broadbent et al., 2019). Buildings and trees obstruct the sky with implications in long and shortwave radiation fluxes downward and upward that may create unpredictable diurnal and seasonal changes in UHI [K] (Kleerekoper et al., 2012; Yang and Li, 2015). Also, it has been shown that not only trees but also the fractional vegetation coverage on urban surfaces can alter urban temperatures with implications in UHI [K] (Armson et al., 2012). Trees, depending on their height and abundance relative to buildings, could also exert drag and alter flow patterns within the canopy, however, this effect is not as significant as the drag induced by buildings (Krayenhoff et al., 2015). Such complex interactions must be accounted for in successful urban micro-climate models.

1.1 Research Gaps

Numerous studies have focused on high-fidelity urban micro-climate models with high spatio-temporal flow resolution, capturing important features of the urban micro-climate with acceptable accuracy (Gowardhan et al., 2011; Soulhac et al., 2011; Blocken, 2015; Nazarian et al., 2018). Some example ~~Computational Fluid Dynamics (CFD)~~ CFD models of this kind include Open-source Field Operation And Manipulation (OpenFOAM) (Aliabadi et al., 2017, 2018), Parallelized Large-Eddy Simulation Model (PALM) (Maronga et al., 2015; Resler et al., 2017), and ENVI-met (Crank et al., 2018). Despite the advances, however, high-fidelity models capable of resolving three-dimensional flows at micro-scale are not computationally efficient and they are complex to implement for operational applications. As a remedy, lower-dimensional flow urban micro-climate models have been developed with many practical applications in city planning, architecture, and engineering consulting. For example, such bulk flow (single-layer) models as Urban Weather Generator (UWG) calculate the flow dynamics in one point, usually the centre of a hypothetical urban canyon, which is representative of all locations (Mills, 1997; Kusaka et al., 2001; Salamanca et al., 2010; Ryu et al., 2011; Bueno et al., 2012a, 2014). Another bulk flow (single-layer) model is the Canyon Air Temperature (CAT) model, which utilizes standard data from a meteorological station to estimate air temperature in a street

canyon (Erell and Williamson, 2006). The Town Energy Balance (TEB) calculates energy balances for urban surfaces, which is forced by meteorological data and incoming solar radiation in the urban site on top of the modeling domain (Masson et al., 2002). The Temperatures of Urban Facets - 3D (TUF-3D) model calculates urban surface temperatures with the main focus on three-dimensional radiation exchange, but it adopts bulk flow (single-layer) modeling, and it is forced by meteorological data on top of its domain (Krayenhoff and Voogt, 2007). More recently TUF-3D was coupled to an Indoor-Outdoor Building Energy Simulator (TUF-3D-IOBES), but this model adopted a bulk flow (single-layer) parameterization (Yaghoobian and Kleissl, 2012). The multi-layer Building Effect Parametrization-Tree (BEP-Tree) model includes variable building heights, the vertical variation of climate variables and the effects of trees, but it is not linked to a building energy model (Martilli et al., 2002; Krayenhoff, 2014; Krayenhoff et al., 2020). More recently, the BEP model has been coupled to a Building Energy Model (BEP+BEM) but it is forced with meteorological variables from higher altitudes above a city using meso-scale models, instead of ~~near surface~~ near-surface meteorological variables measured outside the city (rural areas). An overview of the literature reveals an apparent paucity of an independent urban micro-climate model that accounts for some spatiotemporal variation of meteorological parameters in the urban environment and considers the effects of trees, building energy, radiation, and the connection to the near-surface rural meteorological conditions measured outside a city, without the need for meso-scale modeling, computationally efficiently and is operationally simple for practical applications.

1.2 Objectives

In this study, we present a new urban micro-climate model, called the Vertical City Weather Generator (VCWG), which attempts to overcome some of the limitations mentioned in the previous section. It resolves vertical profiles of climate variables, such as temperature, wind, specific humidity, and turbulence kinetic energy in relation to urban design parameters. VCWG also includes a building energy model. It allows parametric investigation of design options on urban climate control at multiple heights, particularly if multi-storey building design options are considered. This is a significant advantage over the bulk flow (single-layer) models such as UWG, which only consider one point for flow dynamics inside a hypothetical canyon (Masson, 2000; Kusaka et al., 2001; Dupont et al., 2004; Krayenhoff and Voogt, 2007; Lee and Park, 2008; Bueno et al., 2012a, 2014). The advantages of VCWG are as follows. 1) It does not need to be coupled to a meso-scale weather model because it functions standalone as a micro-climate model. 2) Unlike many UCMs that are forced with climate variables above the urban roughness sublayer (e.g. TUF-3D), VCWG is forced with rural climate variables measured at 2 m (temperature and humidity) and 10 m (wind) above ground level (a.g.l.) that are widely accessible and available around the world, making VCWG highly practical for urban design investigations in different climates. Further, unlike UWG, VCWG uses the Monin-Obukhov similarity theory in the rural area to consider effects of thermal stability and aerodynamic, temperature, and specific humidity roughness lengths to establish vertical profiles of potential temperature and specific humidity. 3) VCWG provides urban climate information in one dimension, i.e. resolved vertically, which is advantageous over bulk flow (single-layer) models. 4) VCWG is coupled with the building energy model using two-way interaction. 5) Unlike UWG, VCWG considers the effect of trees in the urban climate by modelling evapotranspiration (latent heat transfer), sensible heat trasnfer, radiation transfer, drag, and other processes due to trees.

The paper is structured as follows. Section 2 describes the methodology, outlining the components of the VCWG model and their connections: the forcing EnergyPlus[TM] Weather (EPW) dataset, the Rural Model (RM), the one-dimensional vertical diffusion model, the building energy model, and the radiation model. This section also describes the location and details of the BUBBLE field campaign used for model evaluation. Section 3 provides the results and discussion. It starts with the detailed evaluation of VCWG by comparing simulation results with those of the BUBBLE field measurements. Then, results from other explorations, including effects of building dimensions, foliage density, building energy configuration, radiation configuration, seasonal variation, and different climate zones on urban climate are briefly presented with references to the supplementary material. Finally, Sect. 4 is devoted to conclusions and future work. Additional information about the sub-models and equations used are provided in the appendix.

2 Methodology

2.1 Vertical City Weather Generator (VCWG)

Figure 1 shows the VCWG model schematic. VCWG consists of four integrated sub-models: 1) a Rural Model (RM) (Sect. 2.1.2) forces meteorological boundary conditions on VCWG based on Monin-Obukhov similarity theory (Paulson, 1970; Businger et al., 1971; Dyer, 1974) and a soil energy balance model (Bueno et al., 2012a, 2014); 2) an urban one-dimensional vertical diffusion model (Sect. 2.1.3) is used for calculation of the vertical profiles of urban micro-climate variables including potential temperature, wind speed, specific humidity, and turbulence kinetic energy, considering the effect of trees, buildings, and building energy system (e.g. condensers and exhaust stacks). This model was initially developed by Santiago and Martilli (2010) and Simón-Moral et al. (2017), while it was later ingested into another model called the Building Effect Parametrization with Trees (BEP-Tree), considering the effects of trees (Krayenhoff, 2014; Krayenhoff et al., 2015, 2020); 3) a Building Energy Model (BEM) (Sect. 2.1.4) is used to determine the waste heat of buildings imposed on the urban environment. This model is a component of the Urban Weather Generator (UWG) model (Bueno et al., 2012a, 2014); 4) a radiation model with vegetation (Sect. 2.1.5) is used to compute the longwave and shortwave heat exchanges between the urban canyon, trees, and the atmosphere/sky. A summary of this model is provided by Meili et al. (2020) and references within.

The sub-models are integrated to predict vertical variation of urban micro-climate variables including potential temperature, wind speed, specific humidity, and turbulence kinetic energy as influenced by aerodynamic and thermal effects of urban elements including longwave and shortwave radiation exchanges, sensible heat fluxes released from urban elements, cooling effect of trees, and the induced drag by urban obstacles. The RM takes latitude, longitude, dry bulb temperature, relative humidity, dew point temperature, and pressure at $2\,\mathrm{m}$ a.g.l., wind speed and direction at $10\,\mathrm{m}$ a.g.l., down-welling direct shortwave radiation, down-welling diffuse shortwave radiation, down-welling longwave radiation, and deep soil temperature from an EPW file. For every time step, and forced with the set of weather data, the RM then computes a potential temperature profile, a specific humidity profile, friction velocity, and a horizontal pressure gradient as a function of friction velocity, all of which are forced as boundary conditions to the one-dimensional vertical diffusion model in the urban area. The potential temperature and specific humidity are forced as fixed values on top of the domain for the urban vertical diffusion model in the temperature and specific

humidity equations, respectively. The horizontal pressure gradient is forced as a source term for the urban vertical diffusion model in the momentum equation. It must be acknowledged that the model does not consider the horizontal advection from the rural area. The model assumes that the rural site is upwind of the urban site, and the top of the domain is above the urban boundary layer. While forced by the RM, the urban one-dimensional vertical diffusion model is also coupled with the building

5   energy and radiation models. The three models have feedback interaction. The urban one-dimensional vertical diffusion model calculates the flow quantities at the centre of control volumes, which are generated by splitting the urban computational domain into multiple layers within and above the urban canyon (see Fig. 2). The urban domain extends to three times building height that conservatively falls closer to the top of the atmospheric roughness sublayer in the urban area (Santiago and Martilli, 2010; Aliabadi et al., 2017), but within the inertial layer in the rural area, where Monin-Obukhov similarity theory can be applied

10   (Basu and Lacser, 2017). In VCWG, buildings with uniformly-distributed height, equal width, and equal spacing from one another, represent the urban area. The feedback interaction coupling scheme among the building energy model, radiation model, and the urban one-dimensional vertical diffusion model is designed to update the boundary conditions, surface temperatures, and the source/sink terms in the transport equations in successive time step iterations. More details about the sub-models are provided in the subsequent sections and the appendix.
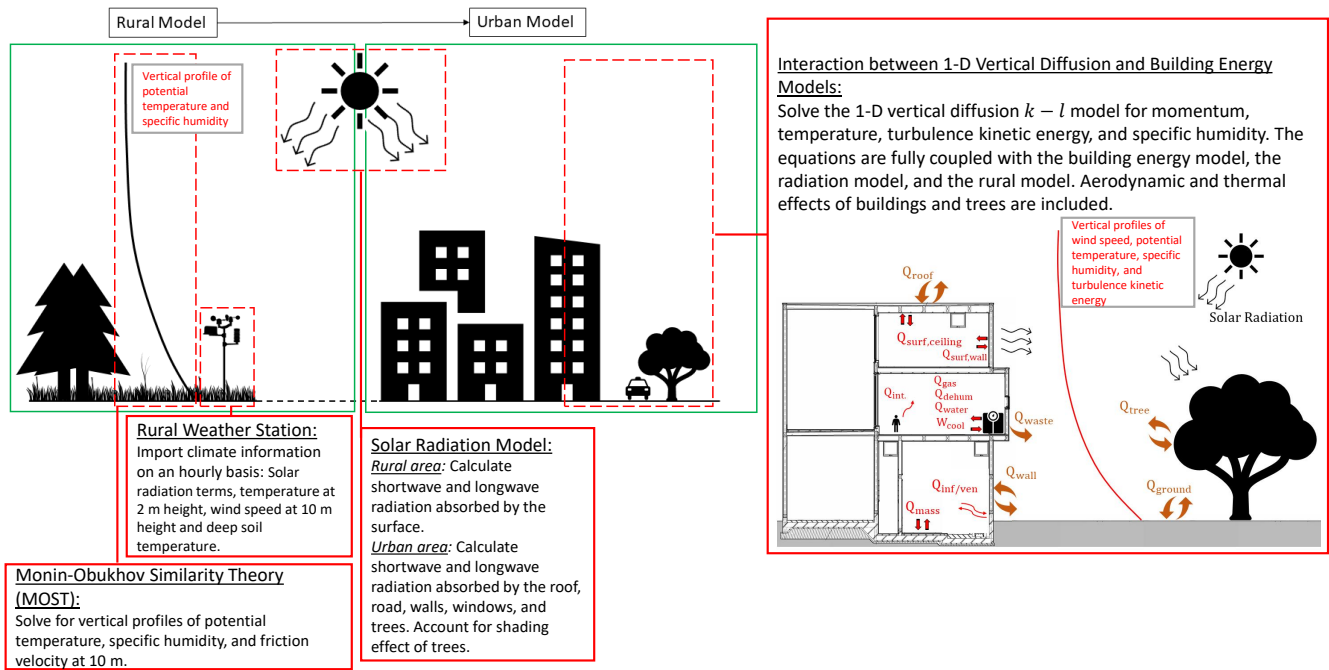
Figure 1. The schematic of Vertical City Weather Generator (VCWG).
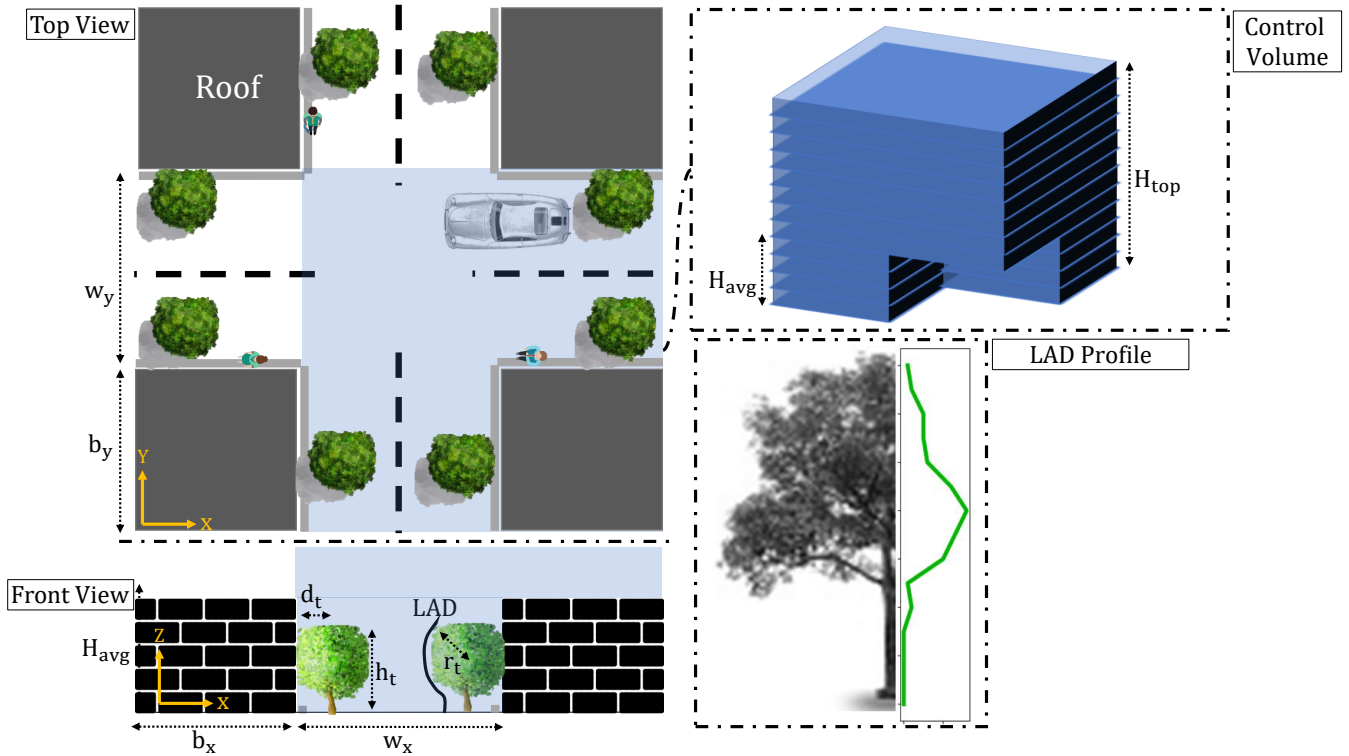
Figure 2. Simplified urban area used in VCWG and corresponding layers of control volumes within and above the canyon. The height of the domain is three times of the average building height. A leaf area density (LAD) $[\text{m}^2\text{m}^{-3}]$ profile is considered to represent trees.

2.1.1 EnergyPlus[TM] Weather Data

Building energy and solar radiation simulations are typically carried out with standardized weather files. EPW files include recent weather data for 2100 locations and are saved in the standard EnergyPlus[TM] format, developed by US department of energy.[1] The data is available for most North American cities, European cities, and other regions around the World. The weather data are arranged by World Meteorological Organization (WMO) based on region and country. An EPW file contains typical hourly-based data of meteorological variables. The meteorological variables are dry bulb temperature, dew point temperature, relative humidity, incoming direct and diffusive shortwave radiation fluxes from the sun and sky, respectively, incoming longwave radiation flux, wind direction, wind speed, sky condition, precipitation (occasionally), deep soil temperature, and general information about field logistics and soil properties. Precipitation data is often missing in the EPW files.

---

[1]https://energyplus.net/weather

2.1.2 Rural Model

In the rural model, the Monin–Obukhov Similarity Theory (MOST) is used to solve for the vertical profiles of potential temperature, specific humidity, and friction velocity at 10 m a.g.l. using meteorological measurements near the surface. MOST is usually applied to the atmospheric surface layer over flat and homogeneous lands to describe the vertical profiles of wind speed, potential temperature, and specific humidity as functions of momentum flux, sensible heat flux, and latent heat flux measured near the surface, respectively. Using MOST the gradient of potential temperature is given by

$$\frac{d\overline{\Theta}_{rur}}{dz} = \frac{Q_{sen,rur}}{\rho C_p \kappa u_* z} \Phi_H\left(\frac{z}{L}\right), \tag{1}$$

where $\overline{\Theta}_{rur}$ [K] is mean potential temperature in the rural area, $Q_{sen,rur}$ [Wm^{-2}] is net rural sensible heat flux, ρ [kgm^{-3}] is air density near the rural surface, C_p [Jkg^{-1}K^{-1}] is air specific heat capacity, u_* [ms^{-1}] is friction velocity, and $\kappa = 0.4$ [-] is the von Kármán constant. Φ_H [-] is known as the universal dimensionless temperature gradient. This term is estimated for different thermal stability conditions based on experimental data by (Businger et al., 1971; Dyer, 1974)

$$\Phi_H\left(\frac{z}{L}\right) = \begin{cases} 1 + 5\frac{z}{L}, & \frac{z}{L} > 0 \text{(Stable)} \\ 1, & \frac{z}{L} = 0 \text{(Neutral)} \\ \left(1 - \frac{16z}{L}\right)^{-1/2}, & \frac{z}{L} < 0 \text{(Unstable)}. \end{cases} \tag{2}$$

In the dimensionless stability parameter z/L [-], z [m] is height above ground and L [m] is Obukhov-Length given by

$$L = \frac{-\overline{\Theta}_{rur,z=2m} u_*^3}{g\kappa \frac{Q_{sen,rur}}{\rho C_p}}. \tag{3}$$

It has been observed that there is a monotonic reduction in friction velocity with increasing stratification (Joffre et al., 2001). So, friction velocity in Eq. 1 is estimated from momentum flux generalization (Monin and Obukhov, 1957)

$$\frac{d\overline{S}_{rur}}{dz} = \frac{u_*}{\kappa z} \Phi_M\left(\frac{z}{L}\right), \tag{4}$$

where $\overline{S}_{rur}$ [ms^{-1}] is the mean horizontal wind speed in the rural area and Φ_M [-] is the universal dimensionless wind shear and is estimated for different thermal stability conditions based on experimental data (Businger et al., 1971; Dyer, 1974)

$$\Phi_M\left(\frac{z}{L}\right) = \begin{cases} 1 + 5\frac{z}{L}, & \frac{z}{L} > 0 \text{(Stable)} \\ 1, & \frac{z}{L} = 0 \text{(Neutral)} \\ \left(1 - \frac{16z}{L}\right)^{-1/4}, & \frac{z}{L} < 0 \text{(Unstable)}. \end{cases} \tag{5}$$

Friction velocity can be determined by integrating Eq. 4, iteratively, over height from the elevation of the rural aerodynamic roughness length z_{0rur} [m] to $z - d_{rur}$ [m], where z=10 m is the reference height for wind measurement and d_{rur} [m] is the zero displacement height. The aerodynamic roughness length and zero displacement height have been rigorously studied and parameterized in the literature as functions of obstacle height h_{rur} [m] and the type of rural area (Raupach et al., 1991;

Hanna and Britter, 2002). VCWG permits this specification, but the approximate ~~values~~ formulations used in this study are $z_{0rur}=0.1h_{rur}$ and $d_{rur}=0.5h_{rur}$. This method provides a friction velocity that is corrected for thermal stability effects.

The potential temperature profiles are also obtained by integration of Eq. 1 (Paulson, 1970) over height from rural roughness length for temperature $z_{\overline{\Theta},rur}$ [m] to $z-d_{rur}$ [m], where z [m] is the desired elevation above ground (here the top of the domain). A typical ~~value of~~ formulation $z_{\overline{\Theta},rur}=0.1z_{0rur}$ [m] is often used (Brutsaert, 1982; Garratt, 1994; Järvi et al., 2011; Meili et al., 2020). This formulation is used in the present study.

Given the similarity of heat and mass transfer (sensible and latent heat fluxes), the same universal dimensionless temperature gradient can be used for the universal dimensionless specific humidity gradient, i.e. $\Phi_Q=\Phi_H$ [-] (Zeng and Dickinson, 1998). The net rural latent heat flux $Q_{lat,rur}$ [Wm^{-2}] can either be directly measured or estimated using the Bowen ratio β_{rur} [-] and the net rural sensible heat flux via $Q_{lat,rur}=Q_{sen,rur}/\beta_{rur}$ [Wm^{-2}]. So the gradient of the specific humidity can be given by the following expression, employing latent heat of vaporization L_v [Jkg^{-1}], as

$$\frac{d\overline{Q}_{rur}}{dz} = \frac{Q_{lat,rur}}{\rho L_v \kappa u_* z}\Phi_Q\left(\frac{z}{L}\right), \tag{6}$$

which can also be integrated over height to give the vertical profile of specific humidity. This expression should be integrated over height from rural roughness length for specific humidity $z_{\overline{Q},rur}$ [m] to $z-d_{rur}$ [m], where z [m] is the desired elevation above ground (here the top of the domain). It is often assumed that $z_{\overline{Q},rur}=z_{\overline{\Theta},rur}$ [m] (Brutsaert, 1982; Järvi et al., 2011; Meili et al., 2020). This assumption is used in the present study.

Meteorological information obtained from the weather station including direct and diffuse shortwave radiation, longwave radiation, temperature at 2 m a.g.l., wind speed at 10 m a.g.l., and deep soil temperature are used to calculate the net rural sensible and latent heat fluxes at the surface via the surface energy balance

$$Q_{S,rur} + Q_{L,rur} = Q_{sen,rur} + Q_{lat,rur} + Q_{grd}, \tag{7}$$

where $Q_{S,rur}$ and $Q_{L,rur}$ [both in Wm^{-2}] are net shortwave and longwave radiation fluxes at the surface (positive with energy flux into the surface) and $Q_{sen,rur}$, $Q_{lat,rur}$, and Q_{grd} [all in Wm^{-2}] are net sensible, latent, and ground heat fluxes at the surface (positive with energy flux leaving the surface). Appendix A details the calculation of each term.

The rural model also outputs a horizontal pressure gradient based on the friction velocity calculation that is later used as a source term for the urban one-dimensional vertical diffusion momentum equation. The pressure gradient is parameterized as $\rho u_*^2/H_{top}$ [kgm^{-2}s^{-2}], where H_{top} [m] is the height of the top of the domain (Krayenhoff et al., 2015; Nazarian et al., 2020), here three times the average building height.

After calculating potential temperature and specific humidity at the top of the domain by the rural model, these values can be applied as fixed-value boundary condition at the top of the domain in the urban one-dimensional vertical diffusion model in the temperature and specific humidity transport equations.

2.1.3 Urban Vertical Diffusion Model

Numerous studies have attempted to parameterize the interaction between urban elements and the atmosphere in terms of dynamical and thermal effects, from very simple models based on MOST (Stull, 1988), to the bulk flow (single-layer) parameterizations (Krayenhoff and Voogt, 2007; Masson, 2000; Kusaka et al., 2001; Bueno et al., 2014), to multi-layer models (Hamdi and Masson, 2008; Santiago and Martilli, 2010; Krayenhoff et al., 2015, 2020) with different levels of complexity. The multi-layer models usually treat aerodynamic and thermal effects of urban elements as sink or source terms in temperature, momentum, specific humidity, and turbulence kinetic energy equations. Parameterization of the exchange processes between the urban elements and the atmosphere can be accomplished using either experimental data or CFD simulations (Martilli et al., 2002; Dupont et al., 2004; Kondo et al., 2005; Kono et al., 2010; Lundquist et al., 2010; Santiago and Martilli, 2010; Krayenhoff et al., 2015; Aliabadi et al., 2019). CFD-based parameterizations proposed by Martilli and Santiago (2007), Santiago and Martilli (2010), Krayenhoff et al. (2015), and Nazarian et al. (2020) use results from Reynolds-Averaged Navier-Stokes (RANS) or Large-Eddy Simulations (LES) including effects of trees and buildings. These parameterizations consider the CFD results at different elevations after being temporally and horizontally averaged.

For the one-dimensional vertical diffusion model, any variable such as cross- and along-canyon wind velocities (U and V $[\mathrm{ms}^{-1}]$, respectively), potential temperature (Θ [K]), and specific humidity (Q $[\mathrm{kgkg}^{-1}]$) is presented using Reynolds averaging. The one-dimensional time-averaged momentum equations in the cross- and along-canyon components can be shown as (Santiago and Martilli, 2010; Krayenhoff, 2014; Krayenhoff et al., 2015; Simón-Moral et al., 2017; Nazarian et al., 2020; Krayenhoff et al., 2020)

$$\frac{\partial \overline{U}}{\partial t} = -\underbrace{\frac{\partial \overline{uw}}{\partial z}}_{I} - \underbrace{\frac{1}{\rho}\frac{\partial \overline{P}}{\partial x}}_{II} - \underbrace{D_x}_{III}, \tag{8}$$

$$\frac{\partial \overline{V}}{\partial t} = -\underbrace{\frac{\partial \overline{vw}}{\partial z}}_{I} - \underbrace{\frac{1}{\rho}\frac{\partial \overline{P}}{\partial y}}_{II} - \underbrace{D_y}_{III}, \tag{9}$$

where $\overline{P}$ [Pa] is time-averaged pressure. The terms on the right hand side of Eqs. 8 and 9 are the vertical gradient of turbulent flux of momentum (I), acceleration due to the large-scale pressure gradient (II), and the sum of pressure, building form, building skin, and vegetation drag terms (III). The parameterization of the latter term is detailed in Appendix A. K-theory is used to parameterize the vertical momentum fluxes, i.e. $\partial \overline{uw}/\partial z = -K_m \partial \overline{U}/\partial z$ and $\partial \overline{vw}/\partial z = -K_m \partial \overline{V}/\partial z$ (the same approach will be used in potential temperature and specific humidity equations), where the diffusion coefficient is calculated using a $\mathrm{k}-\ell$ turbulence model

$$K_m = C_k \ell_k k^{1/2}, \tag{10}$$

where C_k [-] is a constant and ℓ_k [m] is a length scale optimized using sensitivity analysis based on CFD (Nazarian et al., 2020). Note that the plan area density λ_p [-] in this study is greater than the limit considered by Nazarian et al. (2020), so

we assume that the parameterizations extrapolate to this value of λ_p [-]. More details on C_k [-] and ℓ_k [m] are provided in Krayenhoff (2014) and Nazarian et al. (2020). The turbulence kinetic energy k [m^{2}s^{-2}] can be calculated using a prognostic equation (Krayenhoff et al., 2015)

$$\frac{\partial k}{\partial t} = \underbrace{K_m \left[\left(\frac{\partial \overline{U}}{\partial z}\right)^2 + \left(\frac{\partial \overline{V}}{\partial z}\right)^2 \right]}_{I} + \underbrace{\frac{\partial}{\partial z}\left(\frac{K_m}{\sigma_k}\frac{\partial k}{\partial z}\right)}_{II} - \underbrace{\frac{g}{\Theta_0}\frac{K_m}{Pr_t}\frac{\partial \overline{\Theta}}{\partial z}}_{III} + \underbrace{S_{wake}}_{IV} - \underbrace{\varepsilon}_{V}, \tag{11}$$

where g [ms^{-2}] is acceleration due to gravity and Θ_0 [K] is a reference potential temperature. The terms on the right hand side of Eq. 11 are shear production (I), turbulent transport of kinetic energy parameterized based on K-theory (II), buoyant production/dissipation (III), wake production by urban obstacles and trees (IV), and dissipation (V). Parameterizations of the last two terms are presented in more detail in Appendix A and by Krayenhoff (2014). σ_k [-] is the turbulent Prandtl number for turbulence kinetic energy, which is generally suggested to be $\sigma_k=1$ [-] (Pope, 2000).

To calculate the vertical profile of potential temperature in the urban area, the energy transport equation can be derived as

$$\frac{\partial \overline{\Theta}}{\partial t} = \underbrace{\frac{\partial}{\partial z}\left(\frac{K_m}{Pr_t}\frac{\partial \overline{\Theta}}{\partial z}\right)}_{I} + \underbrace{S_{\Theta R} + S_{\Theta G} + S_{\Theta W} + S_{\Theta V} + S_{\Theta A} + S_{\Theta waste}}_{II}, \tag{12}$$

where Pr_t [-] is turbulent Prandtl number, the first term on the right hand side is turbulent transport of heat (I), and the heat sink/source terms (II) correspond to sensible heat exchanges with roof ($S_{\Theta R}$), ground ($S_{\Theta G}$), wall ($S_{\Theta W}$), urban vegetation $S_{\Theta V}$, and radiative divergence $S_{\Theta A}$ [all in Ks^{-1}]. These terms are detailed in appendix A and by Krayenhoff (2014). Contribution of the waste heat emissions from building Heating Ventilation and Air Conditioning (HVAC) system $S_{\Theta waste}$ [Ks^{-1}] is parameterized by

$$S_{\Theta waste} = F_{st}\frac{1}{\rho C_p \Delta z}Q_{HVAC}, \tag{13}$$

where Q_{HVAC} [Wm^{-2}] is total sensible waste heat released into the urban atmosphere per building footprint area, F_{st} [-] is the fraction of waste heat released at street level, while the remainder fraction $(1-F_{st})$ [-] is released at roof level, and Δz [m] is grid discretization in the vertical direction. Depending on the type of building, waste heat emissions can be released partially at street level and the rest at roof level, which can be adjusted by changing F_{st} [-] from 0 to 1. For the BUBBLE campaign, it is assumed that all waste heat was released at roof level, which is more typical in most energy-retrofitted mid-rise apartments (Christen and Vogt, 2004; Rotach et al., 2005). Term Q_{HVAC} [Wm^{-2}] is calculated by the building energy model as

$$Q_{HVAC} = \underbrace{\underbrace{Q_{surf} + Q_{ven} + Q_{inf} + Q_{int}}_{Q_{cool}} + W_{cool} + Q_{dehum}}_{\text{Cooling waste heat}} + Q_{gas} + Q_{water}, \tag{14}$$

$$Q_{HVAC} = \underbrace{(Q_{surf} + Q_{ven} + Q_{inf} + Q_{int})/\eta_{heat}}_{\underbrace{Q_{heat}}_{\text{Heating waste heat}}} + Q_{dehum} + Q_{gas} + Q_{water}, \qquad (15)$$

under cooling and heating modes, respectively. Under cooling mode Q_{HVAC} [Wm^{-2}] is calculated by adding the cooling demand (Q_{cool} [Wm^{-2}]), consisting of surface cooling demand, ventilation demand, infiltration (or exfiltration) demand, and internal energy demand (lighting, equipment, and occupants), energy consumption of the cooling system ($W_{cool}=Q_{cool}/COP$ [Wm^{-2}]) (accounting for Coefficient of Performance (COP [-])), dehumidification demand (Q_{dehum} [Wm^{-2}]), energy consumption by gas combustion (e.g. cooking) (Q_{gas} [Wm^{-2}]), and energy consumption for water heating (Q_{water} [Wm^{-2}]). Under heating mode, Q_{HVAC} [Wm^{-2}] is calculated by adding the heating waste heat (Q_{heat} [Wm^{-2}]), consisting of surface heating demand, ventilation demand, infiltration (or exfiltration) demand, and internal energy demand (lighting, equipment, and occupants) (accounting for thermal efficiency of the heating system (η_{heat} [-])), dehumidification demand (Q_{dehum} [Wm^{-2}]), energy consumption by gas combustion (e.g. cooking) (Q_{gas} [Wm^{-2}]), and energy consumption for water heating (Q_{water} [Wm^{-2}]).

To complete the urban one-dimensional vertical diffusion model, the transport equation for specific humidity is

$$\frac{\partial \overline{Q}}{\partial t} = \underbrace{\frac{\partial}{\partial z}\left(\frac{K_m}{Sc_t}\frac{\partial \overline{Q}}{\partial z}\right)}_{I} + \underbrace{S_{QV}}_{II}, \qquad (16)$$

where $\overline{Q}$ [kgkg^{-1}] is time-averaged specific humidity. The turbulent transport of specific humidity (I) is parameterized based on K-theory, Sc_t [-] is the turbulent Schmidt number, and source term S_{QV} [KgKg^{-1}s^{-1}] (II) is caused by latent heat from vegetation detailed in appendix A and by Krayenhoff (2014).

2.1.4 Building Energy Model

In this study, the balance equation for convection, conduction, and radiation heat fluxes is applied to all building elements (wall, roof, floor, windows, ceiling, and internal mass) to calculate the indoor air temperature. Then, a sensible heat balance equation, between convective heat fluxes released from indoor surfaces and internal heat gains and sensible heat fluxes from the HVAC system and infiltration (or exfiltration), is solved to obtain the time evolution of indoor temperature as

$$\Psi \rho C_p \frac{dT_{in}}{dt} = \underbrace{Q_{surf} + Q_{ven} + Q_{inf} + Q_{int}}_{Q_{cool/heat}}, \qquad (17)$$

where Ψ [m^{3}m^{-2}] is indoor volume per building footprint area, T_{in} [K] is indoor air temperature, and $Q_{cool/heat}$ [Wm^{-2}] is cooling or heating demand as specified in Eqs. 14 and 15. More details on parameterization of the terms in Eq. 17 can be found in appendix A and by Bueno et al. (2012b).

A similar balance equation can be derived for latent heat to determine the time evolution of the indoor air specific humidity as well as the dehumidification load Q_{dehum} [Wm^{-2}], which is parameterized in Bueno et al. (2012b). Note that energy

consumption by gas combustion (e.g. cooking) Q_{gas} and water heating Q_{water} [both in Wm^{-2}] does not influence indoor air temperature or specific humidity, but such energy consumption sources appear in the waste heat Eqs. 14 and 15. These terms are determined from schedules (Bueno et al., 2012b).

The building energy model is a single-zone model with respect to both the indoor and outdoor (urban canopy) environments. That is, only a single temperature is assumed for indoor air, and only a single potential temperature is assumed for outdoor air by integrating the potential temperature profile over height from the street to roof levels. Further, all wall temperatures are assumed to be uniform with height.

2.1.5 Radiation Model with Vegetation

In VCWG, there are two types of vegetation: ground vegetation cover and trees. Ground vegetation cover fraction is specified by δ_s [-]. Tree vegetation is specified by four parameters: tree height h_t [m], tree crown radius r_t [m], tree distance from canyon walls d_t [m], and Leaf Area Index (LAI) [m^2m^{-2}], which is the vertical integral of the Leaf Area Density (LAD) [m^2m^{-3}] profile. VCWG considers two trees spaced from the walls of the canyon with distance d_t [m]. Trees cannot be higher than the building height. Both types of vegetation are specified with the same albedo α_V [-] and emissivity ε_V [-]. The VCWG user can change these input parameters for different vegetation structures. The radiation model in VCWG is adapted from the model developed by Meili et al. (2020). The net all-wave radiation flux is the sum of the net shortwave and longwave radiation fluxes

$$R_n = S^{\downarrow} - S^{\uparrow} + L^{\downarrow} - L^{\uparrow}, \tag{18}$$

where $S^{\downarrow}$, $S^{\uparrow}$, $L^{\downarrow}$, and $L^{\uparrow}$ [all in Wm^{-2}] represent the incoming shortwave, outgoing shortwave, incoming longwave, and outging longwave radiation fluxes. The incoming shortwave radiation fluxes (direct and diffuse) and the longwave radiation flux from the sky are forced by the EPW file. The absorbed (net) shortwave radiation on surface i is given by

$$S_{n,i} = (1 - \alpha_i)\left(S_i^{\downarrow}\right) = (1 - \alpha_i)\left(S_i^{\downarrow direct} + S_i^{\downarrow diffuse}\right), \tag{19}$$

where α_i is the albedo of the surface and $S_i^{\downarrow direct}$ and $S_i^{\downarrow diffuse}$ [Wm^{-2}] are the direct and diffuse incoming shortwave radiation fluxes to surface i. Here i can be S, G, V, W, or T for sky, ground, ground vegetation, wall, and tree. The amount of direct shortwave radiation received by each urban surface is calculated considering shade effects according to well-established methodologies for the case with no trees (Masson, 2000; Kusaka et al., 2001; Wang et al., 2018) and with trees (Ryu et al., 2016). Sky view factors are used to determine the amount of diffuse shortwave radiation that reaches a surface from the sky. Infinite reflections of diffuse shortwave radiation are calculated within the urban canyon with the use of view factors for each pair of urban surfaces (Wang, 2010, 2014). The absorbed (net) longwave radiation for each surface is calculated by

$$L_{n,i} = \varepsilon_i\left(L_i^{\downarrow} - \sigma T_i^4\right), \tag{20}$$

where ε_i [-] is the emissivity of the surface, $(1-\varepsilon_i)$ [-] is the reflectivity of the surface, $L_i^{\downarrow}$ [Wm^{-2}] is the incoming longwave radiation flux, $\sigma = 5.67 \times 10^{-8}$ $Wm^{-2}K^{-4}$ is the Stefan Boltzmann constant, and T_i [K] is the surface temperature. Infinite reflections of longwave radiation within the urban canyon are considered with the use of reciprocal view factors. These view

factors are derived analytically for the case with no trees (Masson, 2000; Lee and Park, 2008; Wang et al., 2013). If trees are present, the view factors are calculated with a simplified two-dimensional Monte Carlo ray-tracing algorithm (Wang, 2014; Frank et al., 2016). More details about the radiation model are provided in appendix A and by Meili et al. (2020).

2.2 Experimental Field Campaigns

5   To evaluate the model, VCWG's predictions are compared to observations from the Basel UrBan Boundary Layer Experiment (BUBBLE) (Christen and Vogt, 2004; Rotach et al., 2005), which was conducted for eight months from December 2001 to July 2002. The urban micro-climate field measurements were conducted in Basel, Switzerland, a typical quasi two-dimensional urban canyon (47.55°N and 7.58°E). An EPW file is used to force the VCWG simulations with rural measurements. The rural measurements correspond to a site 7 km south-east of the city (47.53°N and 7.67°E). The average building height for the urban
10   area is H_{avg}=14.6 m, and the plan area density is λ_p=0.54 [-]. The urban canyon axis is oriented in the northeast-southwest direction with canyon axis angle of θ_{can}=65°. The x and y directions are set to be cross- and the along-canyon, respectively. The frontal area density is λ_f=0.37 [-]. In BUBBLE, wind speed was measured at $z = 3.6, 11.3, 14.7, 17.9, 22.4$, and 31.7 m a.g.l.; potential temperature was measured at $z = 2.6, 13.9, 17.5, 21.5, 25.5$, and 31.2 m a.g.l.; and relative humidity was measured at $z = 2.6$ and 25.5 m a.g.l. The dataset provides the measurements averaged every 10 min. The model predictions
15   of air temperature, wind speed, and specific humidity are compared to the observations on an hourly basis.

3   Results and Discussion

In this section, first the VCWG model results are evaluated against micro-climate field measurements. Next, the model performance is explored by various parametric simulations. A uniform Cartesian grid with 2 m vertical resolution is used. The flow is assumed to be pressure-driven with the pressure gradient of $\rho u_*^2/H_{top}$ [kgm^{-2}s^{-2}], which is decomposed into the x and y
20   directions based on the wind angle ~~. In this equation, the adjustment for wind angle is made based on canyon orientationand the incoming wind angle at the top of the domain~~and canyon orientation. This pressure gradient is forced as source terms on the momentum Eqs. 8 and 9. The boundary condition for potential temperature and specific humidity equations (Eqs. 12 and 16) are determined from the rural model (see Fig. 1). Thus, the VCWG is aimed to calculate momentum~~and~~, temperature, specific humidity, and turbulence kinetic energy exchanges for the centre of each cell in the vertical direction based on the boundary
25   conditions obtained from the rural model, the building energy model, and the radiation model.

3.1 Detailed Model-Observation Comparison

3.1.1 Model Input Variables

The results of the VCWG are compared to the measured data from the BUBBLE campaign. The input parameters representing the urban area are listed in Table 1. The input parameters are inferred from variables, datasets, and simulation codes in the
30   literature that pertain to the BUBBLE campaign and associated models as well as general assumptions found in the literature

Table 1. List of input parameters used in VCWG for model evaluation; input variables are extracted from assumptions, datasets, and simulation codes available from Raupach et al. (1991), Garratt (1994), Hanna and Britter (2002), Christen and Vogt (2004), Järvi et al. (2011) Bueno et al. (2012a), Faroux et al. (2013), Ryu et al. (2016), Yang et al. (2017), Meili et al. (2020), and Mussetti et al. (2020).

Parameter	Source	Symbol	Value
Latitude [°N]	Christen and Vogt (2004)	lat	47.55
Longitude [°E]	Christen and Vogt (2004)	lon	7.58
Average buildings height [m]	Christen and Vogt (2004)	H_{avg}	14.6
Width of canyon [m]	Christen and Vogt (2004)	$w_x=w_y=w$	18.2
Building width to canyon width ratio [-]	Christen and Vogt (2004)	$b_x/w_x=b_y/w_y=b/w$	1.1
Leaf Area Index [$m^2 m^{-2}$]	Faroux et al. (2013), Yang et al. (2017), Mussetti et al. (2020)	LAI	0-1
Tree height [m]	Ryu et al. (2016)	h_t	8
Tree crown radius [m]	Ryu et al. (2016)	r_t	2.5
Tree distance from wall [m]	Ryu et al. (2016)	d_t	3
Ground vegetation cover fraction	Ryu et al. (2016)	δ_s	0
Building type	Christen and Vogt (2004), Bueno et al. (2012a)	-	Mid rise apartment
Urban albedos (roof, ground, wall, vegetation)	Bueno et al. (2012a), Ryu et al. (2016)	$\alpha_R, \alpha_G, \alpha_W, \alpha_V$	0.15, 0.15, 0.15, 0.2
Urban emissivities (roof, ground, wall, vegetation)	Bueno et al. (2012a), Ryu et al. (2016)	$\varepsilon_R, \varepsilon_G, \varepsilon_W, \varepsilon_V$	0.95, 0.95, 0.95, 0.95
Rural overall albedo	Bueno et al. (2012a)	α_{rur}	0.2
Rural overall emissivity	Bueno et al. (2012a)	ε_{rur}	0.95
Rural aerodynamic roughness length [m]	Raupach et al. (1991), Bueno et al. (2012a)	$z_{0rur}=0.1h_{rur}$	0.2
Rural roughness length for temperature [m]	Garratt (1994), Meili et al. (2020)	$z_{\overline{\Theta},rur}=0.1z_{0rur}$	0.02
Rural roughness length for specific humidity [m]	Järvi et al. (2011), Meili et al. (2020)	$z_{\overline{Q},rur}=0.1z_{0rur}$	0.02
Rural zero displacement height [m]	Hanna and Britter (2002)	$d_{rur}=0.5h_{rur}$	1
Rural Bown ratio [-]	Christen and Vogt (2004)	β_{rur}	0.9
Ground aerodynamic roughness length [m]	Bueno et al. (2012a)	z_{0G}	0.02
Roof aerodynamic roughness length [m]	Bueno et al. (2012a)	z_{0R}	0.02
Vertical resolution [m]	-	Δz	2
Time step [s]	-	Δt	60
Canyon axis orientation [°N]	Christen and Vogt (2004)	θ_{can}	65

(Raupach et al., 1991; Garratt, 1994; Hanna and Britter, 2002; Christen and Vogt, 2004; Järvi et al., 2011; Bueno et al., 2012a; Faroux et al., 2013; Ryu et al., 2016; Yang et al., 2017; Meili et al., 2020; Mussetti et al., 2020). In this table, note that the choices of average building height H_{avg}=14.6 [m], street width w=18.2 [m], and building width to street width ratio b/w=1.1 [-] provide λ_p=b/(w+b)=0.52 [-] and λ_f=H_{avg}/(w+b)=0.38 [-], which are remarkably close to morphometric variables reported by Christen and Vogt (2004). The simulations are conducted for eight months from December 2001 to July 2002. Usually the first 24 hours of each month are treated as the model spin-up period. For analysis of each month, the simulation time is approximately 1 min, however it can vary slightly depending on the grid spacing and time step.

3.1.2 Potential Temperature

To compare VCWG results with measured meteorological variables from the BUBBLE campaign, the BIAS, Root Mean Square Error (RMSE), and coefficient of determination R^2 are computed for pairs of model versus observed values every hour for available altitudes and months. This analysis is performed for wind speed, potential temperature, and specific humidity.

5   Figure 3 and Table 2 show the scatter plots of the observed versus simulated values of potential temperature as well as the statistical metrics used for the comparison. Over all altitudes and months, on average, the BIAS, RMSE, and R^2 for potential temperature are 0.25 K, 1.41 K, and 0.82, respectively. These statistics are comparable to what has been reported in the literature for similar models that were compared against observations. For instance, Lauwaet et al. (2016) reported BIAS, RMSE, and R^2 of 0.76 K, 1.32 K, and 0.88, respectively, near ground by comparing model and observation values in a summer.

10   Meili et al. (2020) reported BIAS, RMSE, and R^2 of -0.1 K, 2.2 K, and 0.98, respectively, near ground by comparing model and observation values in a full year. Mussetti et al. (2020) reported BIAS, RMSE, and R^2 of 0.40 K, 1.53 K, and 0.95, respectively, near ground by comparing model and observation values in a summer. Ryu et al. (2016) reported BIAS and RMSE of 0.67 K and 0.99 K, respectively, near ground by comparing model and observation values in a summer. Bueno et al. (2012a) ~~reports~~ reported average BIAS and RMSE of 0.6 K and 0.9 K near the ground for June 2002. VCWG predicts the

15   BIAS, RMSE, and R^2 of -0.1 K, 0.72 K, and 0.95, respectively, near the ground. This comparison reveals that the BIAS and RMSE are improved compared to the predecessor UWG model.
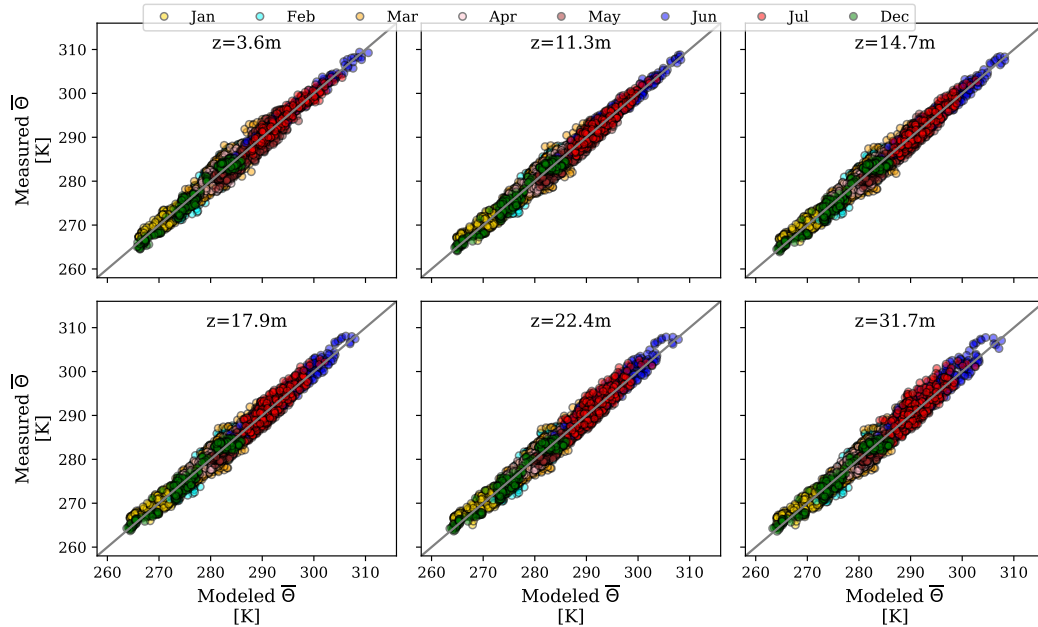
Figure 3. Scatter plots of observed (BUBBLE) versus simulated (VCWG) values of potential temperature for different altitudes and months; each data point corresponds to a 1-hour comparison between the model and observation.

Table 2. BIAS [K], RMSE [K], and R^2 [-] for VCWG predictions of potential temperature against the BUBBLE observations for different altitudes and months.

Altitude z [m]	Statistic	Dec.	Jan.	Feb.	Mar.	Apr.	May	Jun.	July	Average
3.6	BIAS [K]	0.35	0.16	0.58	0.25	0.78	0.81	-0.1	-0.25	0.32
	RMSE [K]	1.10	1.02	1.78	1.90	1.72	1.59	0.72	0.90	1.34
	R^2	0.97	0.70	0.80	0.72	0.62	0.89	0.95	0.88	0.82
11.3	BIAS [K]	0.11	-0.19	0.60	0.23	0.50	0.87	-0.22	-0.23	0.21
	RMSE [K]	1.07	1.17	1.7	1.84	1.59	1.34	0.79	0.96	1.31
	R^2	0.97	0.68	0.81	0.69	0.68	0.90	0.93	0.86	0.81
14.7	BIAS [K]	0.20	-0.22	0.70	0.34	0.57	1.03	-0.12	-0.16	0.29
	RMSE [K]	1.16	1.25	1.78	1.84	1.57	1.33	0.97	1.11	1.38
	R^2	0.96	0.66	0.81	0.70	0.71	0.89	0.92	0.87	0.82
17.9	BIAS [K]	0.26	-0.21	0.75	0.36	0.55	0.99	-0.35	-0.35	0.25
	RMSE [K]	1.19	1.27	1.82	1.85	1.54	1.30	1.14	1.31	1.43
	R^2	0.96	0.68	0.81	0.69	0.73	0.90	0.93	0.86	0.82
22.4	BIAS [K]	0.29	-0.22	0.77	0.38	0.56	0.99	-0.45	-0.42	0.24
	RMSE [K]	1.20	1.30	1.85	1.88	1.50	1.30	1.29	1.49	1.48
	R^2	0.96	0.68	0.81	0.68	0.74	0.90	0.93	0.86	0.82
31.7	BIAS [K]	0.28	-0.28	0.78	0.37	0.58	0.95	-0.64	-0.57	0.18
	RMSE [K]	1.17	1.35	1.87	1.90	1.52	1.31	1.43	1.69	1.53
	R^2	0.96	0.67	0.81	0.65	0.68	0.89	0.93	0.84	0.81
Average	BIAS [K]	0.25	-0.16	0.70	0.32	0.59	0.94	-0.31	-0.33	0.25
	RMSE [K]	1.15	1.23	1.8	1.87	1.57	1.36	1.06	1.24	1.41
	R^2	0.96	0.68	0.81	0.69	0.69	0.90	0.93	0.86	0.82

Figure 4 shows the diurnal variation of the observed versus simulated values of potential temperature averaged for every hour of the day for the available months. The diurnal patterns in temperature reveal that the model has a similar ~~level of success~~ skill in predicting the potential temperature at all hours in lower elevations (z=3.6 to 14.7 m). This performance is comparable to other models that show a ~~well-behaved~~ well-captured diurnal variation of potential temperature at low altitudes (Bueno et al., 2012a; Krayenhoff et al., 2020; Meili et al., 2020; Mussetti et al., 2020). However the diurnal pattern in temperature can deviate between the model and observations at higher elevations (z=17.9 to 31.7 m), especially during midday hours. This can be attributed to more complex flow patterns in the above-roof-level space due to heat advection, horizontal heterogeneity of the urban site, and the above-roof-level shear layer.
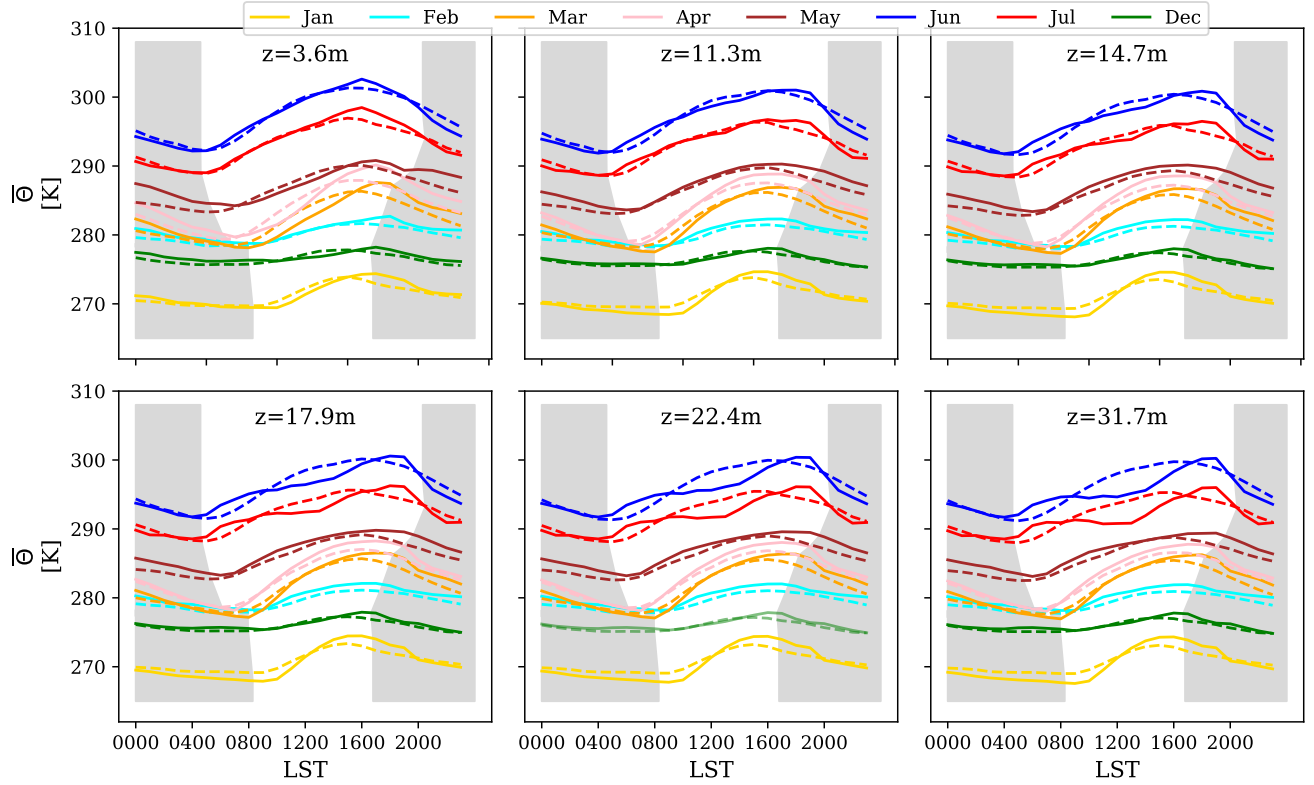
Figure 4. Comparison between the observed (BUBBLE) versus simulated (VCWG) values of potential temperature; the hourly means are shown; nighttime indicated with shaded regions; solid line: model and dashed line: observation; times in Local Standard Time (LST).

3.1.3 Wind Speed

Figure 5 and Table 3 show the scatter plots of the observed versus simulated values of wind speed as well as the statistical metrics used for the comparison. Considering all altitudes and months, the average BIAS, RMSE, and R^2 are 0.67 ms^{-1}, 1.06 ms^{-1}, and 0.41, respectively. Although the comparison reveals a reasonable BIAS and RMSE, the R^2 is lower than values reported for comparisons of potential temperature and specific humidity. This can be explained by the fact that the urban morphology is highly heterogeneous, the measurement of wind is location specific, and that the wind speed and direction can change considerably within each hour. Heterogeneous urban morphology results in great spatial variability of the components of wind velocity vector as a function of wind direction and wind speed (Klein and Clark, 2007; Klein and Galvez, 2015; Afshari and Ramirez, 2021). On the other hand, forced by hourly rural measurements, VCWG assumes a regular urban morphology and predicts the volume-averaged horizontal wind velocity components. So it is expected to obtain lower R^2 values. Other models also often report lower R^2 values for wind speed compared to potential temperature and specific humidity (Mussetti et al., 2020). Overall our BIAS, RMSE, and R^2 values are in agreement with values reported in the literature. For instance,

Lemonsu et al. (2012) reported a range in BIAS of -0.16 to 0.56 ms^{-1}. They also reported a range in RMSE of 0.40 to 0.69 ms^{-1}. Mussetti et al. (2020) reported the BIAS, RMSE, and R^2 of 0.61 ms^{-1}, 1.31 ms^{-1}, and 0.70, respectively.
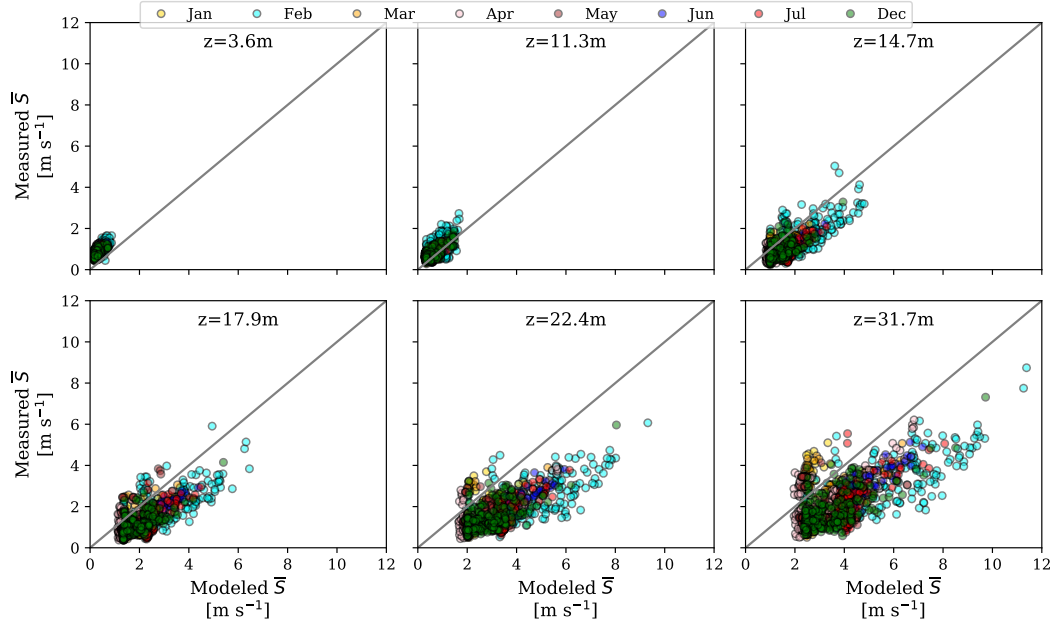
Figure 5. Scatter plots of observed (BUBBLE) versus simulated (VCWG) values of wind speed for different altitudes and months; each data point corresponds to a 1-hour comparison between the model and observation.

3.1.4 Specific Humidity

Figure 6 and Table 4 show the scatter plots of the observed versus simulated values of specific humidity as well as the statistical metrics used for the comparison. Note that specific humidity data were only available in June-July 2002. Over all altitudes and the available months, on average, the BIAS, RMSE, and R^2 for specific humidity are 0.00057 kgkg^{-1}, 0.0010 kgkg^{-1}, and 0.85, respectively. These statistics are comparable to what has been reported in the literature for similar models that were compared against observations. For instance, Mussetti et al. (2020) reported BIAS, RMSE, and R^2 of -0.00109 kgkg^{-1}, 0.00152 kgkg^{-1}, and 0.74, respectively, above the urban canopy for comparisons of model and observations in summer. Lemonsu et al. (2012) reported a range in BIAS of -0.00116 to -0.0005 kgkg^{-1}. They also reported a range in RMSE of 0.00081 to 0.00172 kgkg^{-1}.

Figure 7 shows the diurnal variation of the observed versus simulated values of specific humidity averaged for every hour of the day for June-July 2002. While the diurnal variation is predicted by the model, some deviations are noted between the model and the observation. The model ~~over predicts the observations~~ overpredicts the values at night, while it ~~under predicts the observations~~ underpredicts the values during mid day, especially at z=25.5 m. This could be due to the assumptions of the rural

Table 3. BIAS [ms^{-1}], RMSE [ms^{-1}], and R^2 [-] for VCWG predictions of wind speed against the BUBBLE observations for different altitudes and months.

Altitude z [m]	Statistic	Dec.	Jan.	Feb.	Mar.	Apr.	May	Jun.	July	Average
	BIAS [ms^{-1}]	-0.5	-0.6	-0.59	-0.49	-0.59	-0.40	-0.51	-0.49	-0.52
3.6	RMSE [ms^{-1}]	0.41	0.49	0.46	0.41	0.47	0.33	0.40	0.40	0.42
	R^2	0.55	0.19	0.59	0.47	0.32	0.07	0.43	0.34	0.37
	BIAS [ms^{-1}]	-0.24	-0.35	-0.43	-0.24	-0.28	-0.38	-0.17	-0.18	-0.28
11.3	RMSE [ms^{-1}]	0.22	0.27	0.38	0.21	0.23	0.35	0.18	0.18	0.25
	R^2	0.55	0.26	0.44	0.5	0.43	0.39	0.29	0.35	0.4
	BIAS [ms^{-1}]	0.69	0.43	0.83	0.55	0.54	0.48	0.88	0.87	0.66
14.7	RMSE [ms^{-1}]	0.53	0.36	0.74	0.46	0.47	0.37	0.74	0.79	0.56
	R^2	0.5	0.29	0.56	0.56	0.47	0.08	0.43	0.48	0.42
	BIAS [ms^{-1}]	0.99	0.65	1.27	0.73	0.72	0.73	1.13	1.15	0.92
17.9	RMSE [ms^{-1}]	0.73	0.56	1.00	0.64	0.63	0.67	0.97	1.08	0.79
	R^2	0.56	0.30	0.52	0.58	0.4	0.21	0.43	0.51	0.44
	BIAS [ms^{-1}]	1.7	0.94	2.3	1.2	1.25	1.23	1.96	1.93	1.56
22.4	RMSE [ms^{-1}]	1.27	0.82	1.83	0.97	0.99	1.03	1.67	1.69	1.29
	R^2	0.51	0.38	0.54	0.52	0.50	0.28	0.4	0.46	0.45
	BIAS [ms^{-1}]	1.96	0.98	2.63	1.24	1.24	1.39	2.10	2.08	1.70
31.7	RMSE [ms^{-1}]	1.50	0.95	2.11	1.18	1.09	1.30	1.78	1.85	1.47
	R^2	0.47	0.14	0.58	0.49	0.41	0.17	0.51	0.47	0.41
	BIAS [ms^{-1}]	0.77	0.34	1.00	0.50	0.48	0.51	0.90	0.89	0.67
Average	RMSE [ms^{-1}]	0.78	0.58	1.09	0.64	0.65	0.68	0.96	1.00	1.06
	R^2	0.52	0.26	0.54	0.52	0.42	0.20	0.42	0.43	0.41

model to generate the vertical profile of specific humidity. In this model the latent heat flux in the rural area is parameterized as a function of the sensible heat flux and a fixed Bowen ratio. However, the Bowen ratio can vary diurnally (Kalanda et al., 1979). This can result in a slight miscalculation of the latent heat flux and a forcing boundary condition for specific humidity on top of the modeling domain.

5   **3.1.5   Urban Heat Island (UHI)**

To compare VCWG results with measured UHI [K] from the BUBBLE campaign, the BIAS, RMSE, and R^2 are computed for pairs of hourly model versus observed values for the available months. UHI [K] for the observation is computed by considering the difference between the temperature measurements inside the canyon at $z = 3.6$ m and those temperatures provided by the EPW dataset. For VCWG, UHI [K] is calculated by considering the difference between the temperature prediction inside the
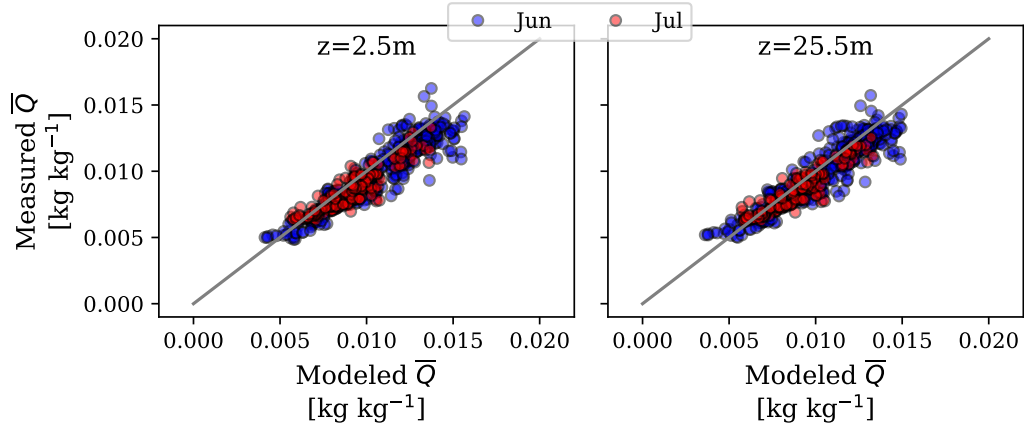
Figure 6. Scatter plots of observed (BUBBLE) versus simulated (VCWG) values of specific humidity for different altitudes and months; each data point corresponds to a 1-hour comparison between the model and observation.

Table 4. BIAS [kgkg^{-1}], RMSE [kgkg^{-1}], and R^2 [-] for VCWG predictions of specific humidity against the BUBBLE observations for different altitudes and months.

Altitude z [m]	Statistic	Jun.	July	Average
	BIAS [kgkg^{-1}]	0.00081	0.00056	0.00069
2.6	RMSE [kgkg^{-1}]	0.0012	0.00086	0.0010
	R^2	0.86	0.84	0.85
	BIAS [kgkg^{-1}]	0.00049	0.00042	0.00045
25.5	RMSE [kgkg^{-1}]	0.0014	0.00074	0.0010
	R^2	0.84	0.86	0.85
	BIAS [kgkg^{-1}]	0.00065	0.00049	0.00057
Average	RMSE [kgkg^{-1}]	0.0013	0.0008	0.0010
	R^2	0.85	0.85	0.85
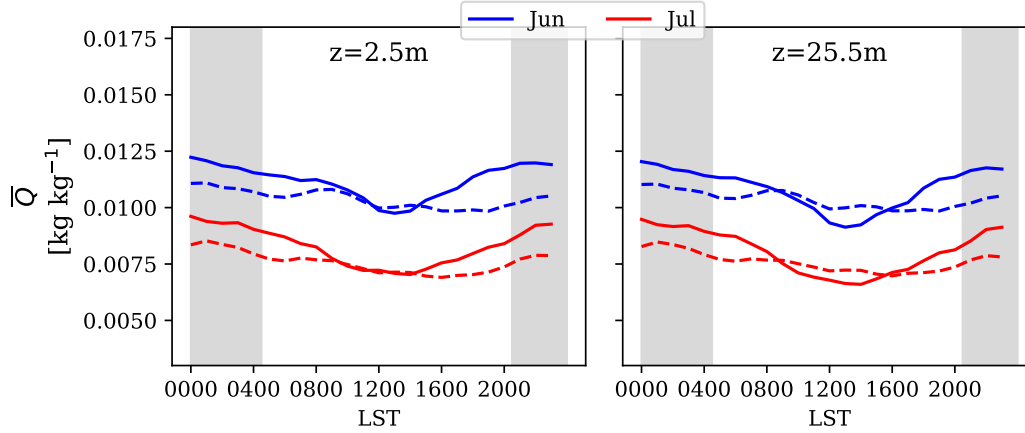
Figure 7. Comparison between the observed (BUBBLE) versus simulated (VCWG) values of specific humidity; the hourly means are shown; nighttime indicated with shaded regions; solid line: model and dashed line: observation; times in Local Standard Time (LST).

Table 5. BIAS [K], RMSE [K], and R^2 [-] for VCWG predictions of UHI [K] against the BUBBLE observations for different months.

Statistic	Dec.	Jan.	Feb.	Mar.	Apr.	May	Jun.	July	Average
BIAS [K]	0.35	0.16	0.58	0.25	0.78	0.81	-0.1	0.06	0.36
RMSE [K]	1.04	0.92	1.63	1.72	1.48	1.42	0.66	0.57	1.2
R^2	0.32	0.37	0.16	0.12	0.50	0.51	0.37	0.47	0.35

canyon at $z = 3$ m and those temperatures provided by the EPW dataset. Figure 8 and Table 5 show the diurnal variation of UHI (for both observations and simulations) as well as the statistical metrics used for the comparison. On average, the BIAS, RMSE, and R^2 for UHI [K] are 0.36 K, 1.2 K, and 0.35, respectively. VCWG predictions of UHI [K] are more successful for months of December, January, April, May, June, and July ($R^2 > 0.3$) than for months of February and March ($R^2 < 0.2$).

5   The deviations in predicting UHI [K] may be attributed to several factors. The heterogeneity of the urban environment and placement of urban sensors may result in sensing slightly warmer or colder temperatures than the spatial average due to the spatial variability of temperature (Mussetti et al., 2020). Also the relative position of the rural site with respect to the urban site, variation of dominant wind directions over different seasons, and horizontal advective transport of heat from the rural area may confound the prediction of UHI. Given that VCWG does not consider all such variations due to simplifying assumptions, it is

10   expected to predict different values of UHI [K] over different seasons in comparison to the observations. Nevertheless, overall, the statistics of UHI [K] comparison are in reasonable agreement with those reported by other models. For example, Mussetti et al. (2020) reported BIAS, RMSE, and R^2 values of -1.88 K, 1.66 K, and 0.55, respectively, for near-ground predictions of UHI [K] in the summer.
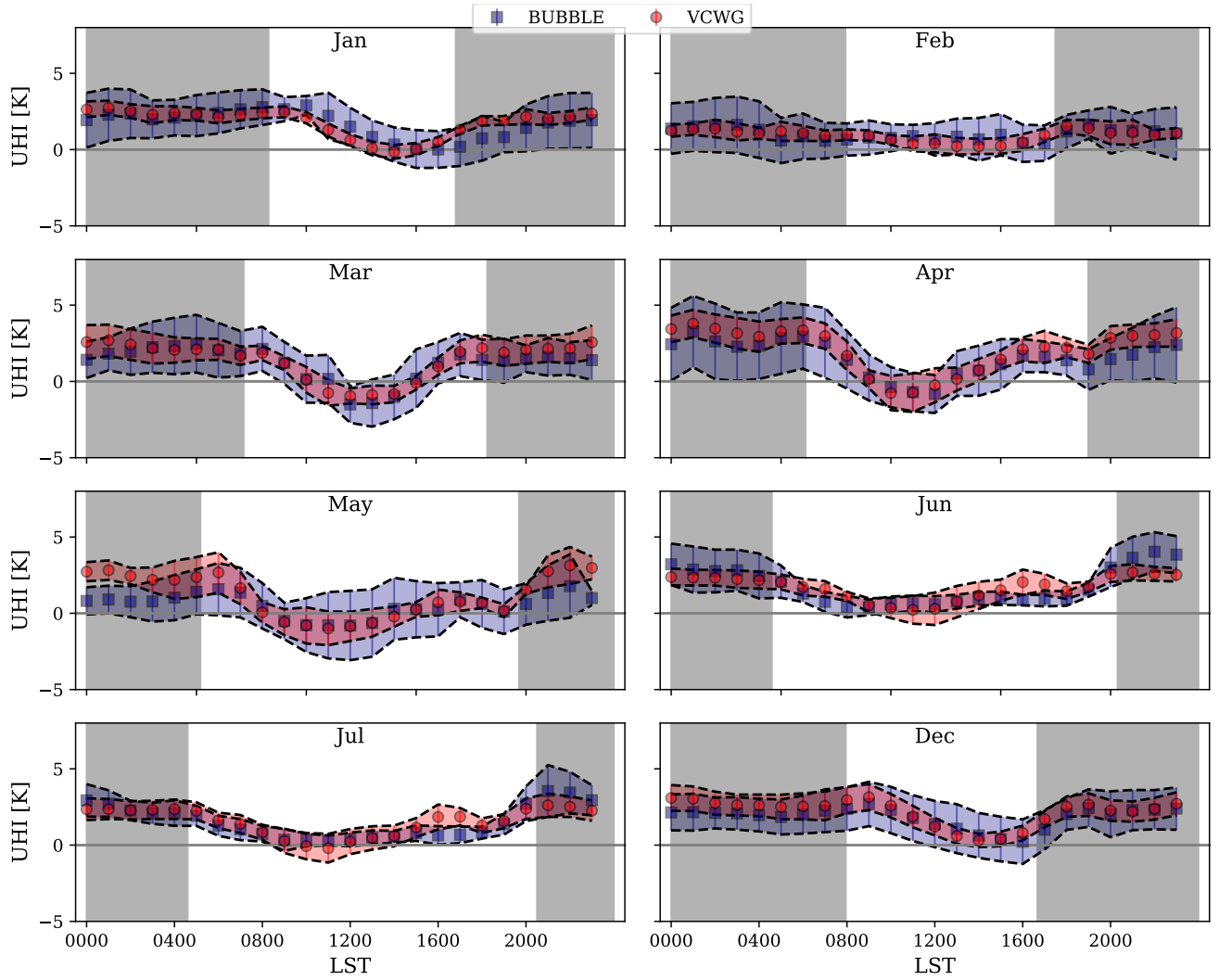
Figure 8. Hourly mean and standard deviation (band) of UHI [K] in each month for the observed (BUBBLE) and predicted (VCWG) values; nighttime indicated with shaded regions; times in Local Standard Time (LST).

3.2 Model Exploration and Comparison with Limited UHI Observations

In this section we explore the capability of the VCWG model to predict urban climate for investigations of the effects of building dimensions, urban vegetation, building energy configuration, radiation configuration, seasonal variations, and other climates. These results are reported in the supplementary material in detail. Here only brief references to the analysis are made. Many explorations consider both nighttime and daytime urban micro-climate. First, we investigate how the urban geometry, which is characterized by plan area density λ_p [-] and frontal area density λ_f [-], can affect the urban micro-climate. An increase in λ_p from 0.46 to 0.54 [-] is associated with lower air temperatures (due to shading) and reduces wind speed within the urban canyon during daytime (see Fig. S1). An increase in λ_f from 0.37 to 0.51 [-] also increases shading effects and consequently reduces daytime temperatures, but it increases nighttime temperatures due to more heat released from urban surfaces that is trapped in the canyon (see Fig. S2). The cooling effect of the urban vegetation is also evaluated by changing the Leaf Area Density (LAD [$m^2 m^{-3}$]) profiles within the canyon. Increasing the average LAD from 0.1 to 0.2 [$m^2 m^{-3}$] shows heat removal from the canyon alongside with lower wind speed due to the drag induced by trees (see Fig. S3). VCWG simulations are also conducted for different building types (a mid-rise apartment and a hospital), cooling system Coefficient of Performance COP [-], heating thermal efficiency η_{heat} [-], and location of building waste heat release F_{st}. The results show that a hospital generates more waste heat fluxes associated with cooling and gas consumption, which increase urban temperatures (see Fig. S4). The analysis of different cooling and heating systems also reveals that less-efficient systems (lower COP from 3.13 to 1 [-] and η_{heat} from 0.8 to 0.4 [-]) result in more waste heat emission and slightly higher temperatures (see Fig. S5). It is found that releasing building waste heat at street level contributes to a higher UHI [K], by 1 K, than releasing the waste heat at roof level (see Fig. S6). This can be due to more effective heat removal from the urban roughness sublayer when the heat is released at roof level. The radiation model is assessed by VCWG simulations for different canyon aspect ratios and axis angles. The radiation fluxes at the road and walls show differences according to canyon aspect ratio and axis angle, while the fluxes at the tree canopy and roof are less sensitive to the canyon aspect ratio and axis angle (see Figs. S7 and S8). ~~VCWG is also evaluated against the observations of Runnalls and Oke (2000) in Vancouver , for a period from 1991 to 1994, for daily maximum and minimum~~ Performance of VCWG is assessed over different seasons with simulations for Vancouver for an entire year. It is found that early daytime UHI [K] values ~~over an entire year. The average BIAS, RMSE, and for daily maximum and minimum~~ are lower than nighttime values, as expected. Also the greatest UHI [K] ~~are , and , and 0.97, respectively (see Figs~~ values are predicted to occur in August and September (see Fig. S9~~and S10~~). Seasonal variations of the vertical profiles of potential temperature, wind speed, specific humidity, and turbulence kinetic energy reveal that the seasonal variations in potential temperature and specific humidity are higher than those associated with wind speed and turbulence kinetic energy (see Fig. ~~S11~~S10). Finally, the ability of the model to predict UHI ~~ranging from diurnally-averaged values of 1.00 to 1.78~~ [K] in different cities with different climate zones is assessed. The case studies are Buenos Aires, Vancouver, Osaka, and Copenhagen (see Fig. ~~S12~~S11). All exploration results obtained from the VCWG are reasonably consistent with the previous observations in the literature.

4 Conclusions and Future Work

The Vertical City Weather Generator (VCWG) is an urban micro-climate model designed to calculate vertical profiles of meteorological variables including potential temperature, wind speed, specific humidity, and turbulence kinetic energy in an urban area. The VCWG is composed of four sub-models for ingestion of urban parameters and meteorological variables in a rural area (as input and boundary conditions) and prediction of the meteorological variables in a nearby urban area, the building energy performance variables, and the short and longwave radiation transfer processes. VCWG combines elements of several previous models developed by Santiago and Martilli (2010), Bueno et al. (2014), Krayenhoff (2014), Krayenhoff et al. (2015), and Meili et al. (2020) to generate a model with the ability to predict vertical profiles of urban meteorological variables, forced by rural measurements, and with two-way coupling with both building energy and radiation models.

To evaluate VCWG, its predictions of potential temperature, wind speed, and specific humidity are compared to observation of the Basel UrBan Boundary Layer Experiment (BUBBLE) micro-climate field campaign for eight months from December 2001 to July 2002 (Christen and Vogt, 2004; Rotach et al., 2005). The model evaluation indicates that the VCWG predicts vertical profiles of meteorological variables in reasonable agreement with field measurements. The average BIAS, RMSE, and R^2 for potential temperature are 0.25 K, 1.41 K, and 0.82, respectively. The average BIAS, RMSE, and R^2 for wind speed are 0.67 ms^{-1}, 1.06 ms^{-1}, and 0.41, respectively. The average BIAS, RMSE, and R^2 for specific humidity are 0.00057 kgkg^{-1}, 0.0010 kgkg^{-1}, and 0.85, respectively. In addition, the average BIAS, RMSE, and R^2 for Urban Heat Island (UHI) are 0.36 K, 1.2 K, and 0.35, respectively. Based on the evaluations, the model performance is comparable to the performance of similar models. The performance of the model is further explored to investigate the effects of urban configurations such as plan and frontal area densities, varying levels of vegetation, building energy configuration, radiation configuration, seasonal variations, and different climate zones on the model predictions. The exploration results also show acceptable performance in agreement with known urban physical processes and observations.

This study shows that the urban micro-climate model VCWG can successfully extend the spatial dimension of the preexisting bulk flow (single-layer) urban micro-climate models to one-dimension in the vertical direction, while it also considers the relationship of the urban micro-climate model to the rural meteorological measurements and the building energy conditions. The effect of the key urban elements such as building configuration, building energy systems (e.g. location of condensers and exhaust stacks), surface vegetation, and trees are considered, but there is still opportunity to improve VCWG further. The urban site is simplified as blocks of buildings with symmetric and regular dimensions, which can be more realistically represented if more considerations are to be taken into account about nonuniform distribution of building dimensions. Also the building energy model in VCWG is a single-zone model, assuming a uniform temperature with height in both indoor and outdoor environments. This limitation can be overcome by improving the radiation model, urban vertical diffusion model, and the building energy model so that wall and indoor temperatures can vary with height, allowing the development of a multi-zone building energy model. In addition, the horizontal advection from the rural area can be considered and parameterized in future work. Future studies can also focus on improvement of flow-field parameterization or including additional source/sink terms in the transport equations to model horizontal motions, eddies, and flow fluctuations in the urban area, which is realistically

very three-dimensional and heterogeneous. Urban hydrology can be added to VCWG in the future to account for precipitation effects. At present, the developed VCWG model can account for the spatial variation of urban micro-climate in a computationally efficient manner independent of an auxiliary meso-scale model. This advantage is really important for urban planners, architects, and consulting engineers, for operationally-fast VCWG simulations.

5 *Code and data availability.* The VCWG v1.3.0 is developed at the Atmospheric Innovations Research (AIR) Laboratory at the University of Guelph: http://www.aaa-scientists.com. The source code is available under GPL 3.0 licence: https://opensource.org/licenses/GPL-3.0 (last access: October 2020) and can be downloaded from https://www.zenodo.org/ with DOI: 10.5281/zenodo.4255225.

Appendix A

A1 Surface Energy Balance in the Rural Area

10 In Eq. 7 the net shortwave solar radiation flux absorbed at the surface can be calculated from

$$Q_{S,rur} = ((1 - F_{veg})(1 - \alpha_{rur}) + F_{veg}(1 - \alpha_V))(S^{\downarrow direct} + S^{\downarrow diffuse}), \tag{A1}$$

where F_{veg} [-] is the fraction of the rural area covered by vegetation, α_{rur} [-] is overall albedo of the rural area, α_V [-] is the albedo of vegetation (here considered to be the same for rural and urban vegetation), and $S^{\downarrow direct}$ and $S^{\downarrow diffuse}$ [Wm^{-2}] are the forcing direct and diffuse shortwave radiation fluxes from the EPW file, respectively. The net longwave solar radiation flux

15 absorbed at the surface can be calculated from

$$Q_{L,rur} = L^{\downarrow} - L^{\uparrow} = \varepsilon_{rur}\left(L^{\downarrow} - \sigma T_{s,rur}^4\right), \tag{A2}$$

where $L^{\downarrow}$ [Wm^{-2}] is the forcing longwave radiation flux from the EPW file, $L^{\uparrow}$ [Wm^{-2}] is the longwave radiation flux leaving the rural surface at temperature $T_{s,rur}$ [K], and ε_{rur} [-] is rural surface emissivity. The net sensible heat flux is calculated using Louis (1979)

20 $$Q_{sen,rur} = \rho C_p \frac{\kappa^2}{\left(\ln \frac{z}{z_{0rur}}\right)^2} \frac{1}{R} \overline{S}_{rur,z=10m}\left(\overline{\Theta}_{rur,s} - \overline{\Theta}_{rur,2m}\right) F_h\left(\frac{z}{z_{0rur}}, Ri_B\right), \tag{A3}$$

where R [-] is a model constant, Ri_B [-] is the bulk Richardson number, and F_h [-] is the stability function for sensible heat flux defined by Louis (1979). The net latent heat flux is calculated using the Bowen ratio β_{rur} [-] such that $Q_{lat,rur} = Q_{sen,rur}/\beta_{rur}$ [Wm^{-2}]. The ground heat flux drives the conduction equation at the upper-most soil layer via (Bueno et al., 2012a)

$$dC_v \frac{dT_1}{dt} = C(T_2 - T_1) + Q_{grd}, \tag{A4}$$

25 where d [m] is the soil layer thickness, C_v [Jm^{-3}K^{-1}] is volumetric heat capacity of soil, $T_1 = \overline{\Theta}_{rur,s}$ [k] is soil upper layer temperature (the same as soil surface temperature), C [Wm^{-2}K^{-1}] is the soil thermal conductance, and T_2 [K] is soil

temperature in the second layer under ground. In the lowest layer (n) of soil the conduction equation is forced by a deep soil temperature T_{deep} [K]

$$dC_v \frac{dT_{n-1}}{dt} = C(T_{deep} - T_{n-1}). \tag{A5}$$

A2   Source/Sink Term in the 1-D Model

5   The pressure and skin drags exerted on the flow in Eqs. 8 and 9 are formulated as follows (Santiago and Martilli, 2010; Krayenhoff, 2014; Krayenhoff et al., 2015; Simón-Moral et al., 2017; Nazarian et al., 2020; Krayenhoff et al., 2020)

$$D_x = \underbrace{\frac{1}{\rho}\frac{\partial \tilde{P}}{\partial x}}_{I} + \underbrace{\nu(\nabla^2 \tilde{U})}_{II}, \tag{A6}$$

$$D_y = \underbrace{\frac{1}{\rho}\frac{\partial \tilde{P}}{\partial y}}_{I} + \underbrace{\nu(\nabla^2 \tilde{V})}_{II}, \tag{A7}$$

where term I represents dispersive pressure variation (form drag) induced by vegetation and building and term II represents
10   the dispersive viscous dissipation (skin drag) induced by horizontal surfaces. The former can be parameterized as

$$\frac{1}{\rho}\frac{\partial \tilde{P}}{\partial x} = \left(B_D C_{DBv} + LAD\Omega C_{DV}\right)\overline{U}_{expl}\overline{U}, \tag{A8}$$

$$\frac{1}{\rho}\frac{\partial \tilde{P}}{\partial y} = \left(B_D C_{DBv} + LAD\Omega C_{DV}\right)\overline{V}_{expl}\overline{V}, \tag{A9}$$

where B_D [m^{-1}] is sectional building area density, C_{DBv} [-] is sectional drag coefficient in the presence of trees, LAD [m^{2}m^{-3}] is leaf area density in the canyon, Ω [-] is clumping factor, C_{DV} [-] is the drag coefficient for tree foliage, and $\overline{U}_{expl}$
15   and $\overline{V}_{expl}$ [ms^{-1}] are wind velocity components in x and y directions from a previous numerical solution, respectively, which are assumed explicitly as constants to linearize the system of equations to be solved. The skin drag can be parameterized as follows

$$\nu(\nabla^2 \tilde{U}) = \frac{1}{\Delta z}c_d f_m \overline{U}_{expl}\overline{U}, \tag{A10}$$

$$\nu(\nabla^2 \tilde{V}) = \frac{1}{\Delta z}c_d f_m \overline{V}_{expl}\overline{V}, \tag{A11}$$

20   where c_d [-] is skin drag coefficient and f_m [-] is a function of stability from Louis (1979). The terms related to wake production S_{wake} and dissipation rate ε [both in m^{2}s^{-3}] in Eq. 11 can be parameterized as

$$S_{wake} = \left(B_D C_{DBv} + LAD\Omega C_{DV}\right)\overline{U}^3_{expl}, \tag{A12}$$

$$\varepsilon = C_\varepsilon \frac{k^{\frac{3}{2}}}{\ell_{\varepsilon,dissip}}, \tag{A13}$$

where Ω [-] is clumping factor, C_ε [-] is a model constant and $\ell_{\varepsilon,\text{dissip}}$ [m] is a dissipation length scale obtained by sensitivity
25   study using CFD (Nazarian et al., 2020). Note that plan area density λ_p [-] in this study is greater than the limit considered by

Nazarian et al. (2020), so we assume that the parameterizations extrapolate to this value of λ_p [-]. The heat source/sink terms, terms in Eq. 12, caused by roof ($S_{\Theta R}$) and ground ($S_{\Theta G}$) [both in Ks^{-1}] are calculated based on the study by Louis (1979) and the heat flux from the wall ($S_{\Theta W}$ [Ks^{-1}]) is formulated in Martilli et al. (2002). The two other source/sink terms can be parameterized as below

$$S_{\Theta A} = \frac{4\rho_{abs}k_{air}}{\rho C_p v_L}\left[(1-\lambda_p)L_A\right], \tag{A14}$$

$$S_{\Theta V} = \frac{2g_{Ha}c_{PM}}{\rho C_p v_L}\left[LAD(1-\lambda_p)(\overline{\Theta}_V - \overline{\Theta})\right], \tag{A15}$$

where L_A [Wm^{-2}] is the absorbed flux density of longwave radiation in the canyon, ρ_{abs} [kgm^{-3}] is the density of absorbing molecules, k_{air} [m^2kg^{-1}] is their mass extinction cross section, $v_L=(1-\lambda_p)$ [-] is the fraction of total volume that is outdoor air, g_{Ha} [$molm^{-2}s^{-1}$] is conductance for heat, c_{PM} [$Jmol^{-1}K^{-1}$] is the molar heat capacity for the air, and $\overline{\Theta}_V$ [K] is the temperature of tree foliage. In the specific humidity Eqn. 16, the source/sink term can be calculated using the following equation

$$S_{QV} = \frac{\Lambda_M g_v \Omega}{\rho \Lambda v_L}\left[LAD(1-\lambda_p)\left(s[\overline{\Theta}_V - \overline{\Theta}] + \frac{D}{P}\right)\right] \tag{A16}$$

where Λ_M [$Jmol^{-1}$] is molar latent heat of vaporization, Λ [Jkg^{-1}] is latent heat of vaporization,, g_v [$molm^{-2}s^{-1}$] is the average surface and boundary-layer conductance for humidity for the whole leaf, s [K^{-1}] is derivative of saturation vapour pressure with respect to temperature divided by pressure, D [Pa] is the vapour deficit of the atmosphere, and P [Pa] is atmospheric pressure.

A3 Building Heat Exchanges

The heat fluxes in Eq. 17 can be parameterized as

$$Q_{surf} = \Sigma h_i A_i (T_{si} - T_{in}) \tag{A17}$$

$$Q_{inf} = \dot{m}_{inf} C_p (T_{out} - T_{in}) \tag{A18}$$

$$Q_{vent} = \dot{m}_{vent} C_p (T_{supp} - T_{in}) \tag{A19}$$

where h_i [$Wm^{-2}K^{-1}$] is convective heat transfer coefficient for surface i and A_i [m^2m^{-2}] is surface area for surface i per building foot print area. Surface i can correspond to indoor elements such as ceiling, walls, floor, building mass, and windows. T_{si} [K] is the temperature of the inner layer of elements, T_{in} [K] is indoor temperature, T_{out} [K] is the outdoor temperature averaged over building height, T_{supp} [K] is supply temperature, $\dot{m}_{inf}$ [$kgs^{-1}m^{-2}$] is mass flow rate of infiltration (exfiltration) per building footprint area, and $\dot{m}_{vent}$ [$kgs^{-1}m^{-2}$] is mass flow rate of ventilated air in the HVAC system per building footprint area.

A4   Radiation Model

A summary of details for the radiation model is provided here from Meili et al. (2020). The direct and diffuse shortwave radiation fluxes absorbed by each urban element are computed as functions of urban canyon height, width, tree shape, and albedo. The urban geometry creates shading effects by blocking a portion of the incoming direct solar radiation flux. This flux
5 is further decreased by the sky view factor, which reduces the incoming diffuse solar radiation flux and traps reflected solar rays within the canyon. Two steps are involved to calculate the net shortwave radiation flux: 1a) the direct shortwave radiation flux received by each urban element is calculated as a function of the sun position and shading effects created by buildings and trees; 1b) the diffuse shortwave radiation received by each urban element is computed as a function of the corresponding sky view factor; 2) infinite radiation reflections within the urban canyon are calculated using view factors and the net shortwave radiation
10 flux for each urban element is then calculated. All urban elements are assumed to be Lambertian with isotropic scattering and reflections. If there are no trees, the view factors are computed analytically. Otherwise a Monte Carlo ray tracing algorithm is used. No obstructions are considered for roofs, i.e. trees cannot be taller than buildings. The model computes the net shortwave radiation flux due to both direct and diffuse radiation, allowing to investigate effects of shade and albedo in detail. The energy associated with the shortwave radiation exchange on each urban element is conserved.

15 For net longwave radiation flux on each urban surface, the difference between the incoming and outgoing longwave radiation fluxes are considered. These fluxes depend on surface temperatures. Infinite reflections of longwave radiation within the urban canyon are considered. Again, no obstructions are considered for roofs, i.e. trees cannot be taller than buildings. The canyon air does not impact the radiation exchange. The energy associated with the longwave radiation exchange on each urban surface is conserved.

20 For the case of no trees, analytical view factors are calculated using standard equations (Masson, 2000; Lee and Park, 2008; Ryu et al., 2011; Wang et al., 2013), while for trees the method of Ryu et al. (2016) is used. View factors meet a set of three requirements: 1) the self view factor of a flat surface is zero, 2) energy at the surface is conserved, and 3) view factors are reciprocal. The view factors for the case with trees are calculated using a Monte Carlo ray tracing algorithm (Wang, 2014; Frank et al., 2016). This algorithm performs a probabilistic sampling of all rays emitted by an urban element. The relative
25 frequency of rays emitted by one element that hit another element is an estimation of the view factor between the two elements. On each element, a large number of randomly distributed emitting points are considered. These view factors are also corrected for the three requirements mentioned above.

Author contributions. MM wrote the paper with significant conceptual input from ESK and AAA and critical feedback from all co-authors. BB and LKN developed the base Urban Weather Generator (UWG) program in MATLAB. CM and SV translated UWG from MATLAB
30 to Python. NN and ESK provided their code for the one-dimensional vertical diffusion model for the urban climate that was integrated into VCWG. MM and AAA developed the Vertical City Weather Generator (VCWG) program in Python by integrating various modeling components developed by BB, LKN, CM, SV, ESK, and NN. BD, AN, MKN, and MRN edited the manuscript.

Competing interests. The authors declare that they have no conflict of interest.

Acknowledgements. The computational platforms were set up with the assistance of Jeff Madge, Joel Best, and Matthew Kent at the University of Guelph. The authors thank Alberto Martilli at Centre for Energy, Environment and Technology (CIEMAT) in Madrid, Spain, who developed and shared an earlier version of the one-dimensional vertical diffusion model for the urban climate. The authors thank Naika
5 Meili at Institute of Environmental Engineering, ETH Zurich, Zurich, Switzerland, who developed and shared an earlier version of the urban radiation model. The authors also thank Andreas Christen at Environmental Meteorology, University of Freiburg, Freiburg, Germany, who provided the observation data from an extended period of the BUBBLE campaign.

This work was supported by the University of Guelph through the International Graduate Tuition Scholarship (IGTS) for the lead author; Discovery Grant program (401231) from the Natural Sciences and Engineering Research Council (NSERC) of Canada; Government of
10 Ontario through the Ontario Centres of Excellence (OCE) under the Alberta-Ontario Innovation Program (AOIP) (053450); and Emission Reduction Alberta (ERA) (053498). OCE is a member of the Ontario Network of Entrepreneurs (ONE).

References

Afshari, A. and Ramirez, N.: Improving the accuracy of simplified urban canopy models for arid regions using site-specific prior information, Urban Climate, 35, 100 722, https://doi.org/10.1016/j.uclim.2020.100722, 2021.

Akbari, H., Pomerantz, M., and Taha, H.: Cool surfaces and shade trees to reduce energy use and improve air quality in urban areas, Sol. Energy, 70, 295–310, https://doi.org/10.1016/S0038-092X(00)00089-X, 2001.

Aliabadi, A. A., Krayenhoff, E. S., Nazarian, N., Chew, L. W., Armstrong, P. R., Afshari, A., and Norford, L. K.: Effects of roof-edge roughness on air temperature and pollutant concentration in urban canyons, Bound.-Lay. Meteorol., 164, 249–279, https://doi.org/10.1007/s10546-017-0246-1, 2017.

Aliabadi, A. A., Veriotes, N., and Pedro, G.: A Very Large-Eddy Simulation (VLES) model for the investigation of the neutral atmospheric boundary layer, J. Wind Eng. Ind. Aerod., 183, 152–171, https://doi.org/10.1016/j.jweia.2018.10.014, 2018.

Aliabadi, A. A., Moradi, M., Clement, D., Lubitz, W. D., and Gharabaghi, B.: Flow and temperature dynamics in an urban canyon under a comprehensive set of wind directions, wind speeds, and thermal stability conditions, Environ. Fluid Mech., 19, 81–109, https://doi.org/10.1007/s10652-018-9606-8, 2019.

Armson, D., Stringer, P., and Ennos, A.: The effect of tree shade and grass on surface and globe temperatures in an urban area, Urban For. Urban Gree., 11, 245–255, https://doi.org/10.1016/j.ufug.2012.05.002, 2012.

Basu, S. and Lacser, A.: A cautionary note on the use of Monin–Obukhov similarity theory in very high-resolution large-eddy simulations, Bound.-Lay. Meteorol., 163, 351–355, https://doi.org/10.1007/s10546-016-0225-y, 2017.

Blocken, B.: Computational Fluid Dynamics for urban physics: Importance, scales, possibilities, limitations and ten tips and tricks towards accurate and reliable simulations, Build. Environ., 91, 219–245, https://doi.org/10.1016/j.buildenv.2015.02.015, 2015.

Bornstein, R. D.: The two-dimensional URBMET urban boundary layer model, J. Appl. Meteorol., 14, 1459–1477, https://doi.org/10.1175/1520-0450(1975)014<1459:TTDUUB>2.0.CO;2, 1975.

Britter, R. E. and Hanna, S. R.: Flow and dispersion in urban areas, Annu. Rev. Fluid Mech, 35, 469–496, https://doi.org/10.1146/annurev.fluid.35.101101.161147, 2003.

Broadbent, A. M., Coutts, A. M., Nice, K. A., Demuzere, M., Krayenhoff, E. S., Tapper, N. J., and Wouters, H.: The Air-temperature Response to Green/blue-infrastructure Evaluation Tool (TARGET v1. 0): an efficient and user-friendly model of city cooling, Geosci. Model Dev., 12, 785–803, https://doi.org/10.5194/gmd-12-785-2019, 2019.

Brutsaert, W.: Evaporation into the atmosphere, Springer, Dordrecht, https://doi.org/10.1007/978-94-017-1497-6, 1982.

Bueno, B., Norford, L. K., Pigeon, G., and Britter, R.: Combining a detailed building energy model with a physically-based urban canopy model, Bound.-Lay. Meteorol., 140, 471–489, https://doi.org/10.1007/s10546-011-9620-6, 2011.

Bueno, B., Norford, L. K., Hidalgo, J., and Pigeon, G.: The urban weather generator, J. Build. Perf. Simulat., 6, 269–281, https://doi.org/10.1080/19401493.2012.718797, 2012a.

Bueno, B., Pigeon, G., Norford, L. K., Zibouche, K., and Marchadier, C.: Development and evaluation of a building energy model integrated in the TEB scheme, Geosci. Model Dev., 5, 433–448, https://doi.org/10.5194/gmd-5-433-2012, 2012b.

Bueno, B., Roth, M., Norford, L. K., and Li, R.: Computationally efficient prediction of canopy level urban air temperature at the neighbour-hood scale, Urban Climate, 9, 35–53, https://doi.org/10.1016/j.uclim.2014.05.005, 2014.

Businger, J. A., Wyngaard, J. C., Izumi, Y., and Bradley, E. F.: Flux-profile relationships in the atmospheric surface layer, J. Atmos. Sci., 28, 181–189, https://doi.org/10.1175/1520-0469(1971)028<0181:FPRITA>2.0.CO;2, 1971.

Chen, F., Kusaka, H., Bornstein, R., Ching, J., Grimmond, C. S. B., Grossman-Clarke, S., Loridan, T., Manning, K. W., Martilli, A., Miao, S., Sailor, D., Salamanca, F. P., Taha, H., Tewari, M., Wang, X., Wyszogrodzki, A. A., and Zhang, C.: The integrated WRF/urban modelling system: development, evaluation, and applications to urban environmental problems, Int. J. Climatol., 31, 273–288, https://doi.org/10.1002/joc.2158, 2011.

5 Chin, H.-N. S., Leach, M. J., Sugiyama, G. A., Leone Jr, J. M., Walker, H., Nasstrom, J., and Brown, M. J.: Evaluation of an urban canopy parameterization in a mesoscale model using VTMX and URBAN 2000 Data, Mon. Weather Rev., 133, 2043–2068, https://doi.org/10.1175/MWR2962.1, 2005.

Christen, A. and Vogt, R.: Energy and radiation balance of a central European city, Int. J. Climatol., 24, 1395–1421, https://doi.org/10.1002/joc.1074, 2004.

10 Crank, P. J., Sailor, D. J., Ban-Weiss, G., and Taleghani, M.: Evaluating the ENVI-met microscale model for suitability in analysis of targeted urban heat mitigation strategies, Urban climate, 26, 188–197, https://doi.org/10.1016/j.uclim.2018.09.002, 2018.

Dupont, S., Otte, T. L., and Ching, J. K. S.: Simulation of meteorological fields within and above urban and rural canopies with a mesoscale model, Bound.-Lay. Meteorol., 113, 111–158, https://doi.org/10.1023/B:BOUN.0000037327.19159.ac, 2004.

Dyer, A. J.: A review of flux-profile relationships, Bound.-Lay. Meteorol., 7, 363–372, https://doi.org/10.1007/BF00240838, 1974.

15 Erell, E. and Williamson, T.: Simulating air temperature in an urban street canyon in all weather conditions using measured data at a reference meteorological station, Int. J. Climatol., 26, 1671–1694, https://doi.org/10.1002/joc.1328, 2006.

Faroux, S., Kaptué Tchuenté, A. T., Roujean, J.-L., Masson, V., Martin, E., and Le Moigne, P.: ECOCLIMAP-II/Europe: a twofold database of ecosystems and surface parameters at 1 km resolution based on satellite information for use in land surface, meteorological and climate models, Geosci. Model Dev., 6, 563–582, https://doi.org/10.5194/gmd-6-563-2013, 2013.

20 Frank, A., Heidemann, W., and Spindler, K.: Modeling of the surface-to-surface radiation exchange using a Monte Carlo method, Journal of Physics: Conference Series, 745, 032 143, 2016.

Garratt, J.: The Atmospheric Boundary Layer, Cambridge University Press, London, 1994.

Gowardhan, A. A., Pardyjak, E. R., Senocak, I., and Brown, M. J.: A CFD-based wind solver for an urban fast response transport and dispersion model, Environ. Fluid Mech., 11, 439–464, https://doi.org/10.1007/s10652-011-9211-6, 2011.

25 Grimmond, C. S. B. and Oke, T. R.: Aerodynamic properties of urban areas derived from analysis of surface form, J. Appl. Meteorol., 38, 1262–1292, https://doi.org/10.1175/1520-0450(1999)038<1262:APOUAD>2.0.CO;2, 1999.

Grimmond, C. S. B., Souch, C., and Hubble, M. D.: Influence of tree cover on summertime surface energy balance fluxes, San Gabriel Valley, Los Angeles, Clim. Res., 6, 45–57, 1996.

Gros, A., Bozonnet, E., and Inard, C.: Cool materials impact at district scale: Coupling building energy and microclimate models, Sustain.
30 Cities Soc., 13, 254–266, https://doi.org/10.1016/j.scs.2014.02.002, 2014.

Hamdi, R. and Masson, V.: Inclusion of a drag approach in the Town Energy Balance (TEB) Scheme: Offline 1D Evaluation in a Street Canyon, J. Appl. Meteorol. Clim., 47, 2627–2644, https://doi.org/10.1175/2008JAMC1865.1, 2008.

Hanna, S. R. and Britter, R. E.: Wind flow and vapor cloud dispersion at industrial and urban sites, American Institute of Chemical Engineers, New York, 2002.

35 Järvi, L., Grimmond, C. S. B., and Christen, A.: The surface urban energy and water balance scheme (SUEWS): Evaluation in Los Angeles and Vancouver, J. Hydrol., 411, 219–237, 2011.

Joffre, S. M., Kangas, M., Heikinheimo, M., and Kitaigorodskii, S. A.: Variability of the stable and unstable atmospheric boundary-layer height and its scales over a Boreal forest, Bound.-Lay. Meteorol., 99, 429–450, https://doi.org/10.1023/A:1018956525605, 2001.

Kalanda, B. D., Oke, T. R., and Spittlehouse, D. L.: Suburban Energy Balance Estimates for Vancouver, B.C., Using the Bowen Ratio-Energy Balance Approach, J. Appl. Meteorol., 19, 791–802, https://doi.org/10.1175/1520-0450(1980)019<0791:SEBEFV>2.0.CO;2, 1979.

Kastner-Klein, P., Berkowicz, R., and Britter, R.: The influence of street architecture on flow and dispersion in street canyons, Meteorol. Atmos. Phys, 87, 121–131, https://doi.org/10.1007/s00703-003-0065-4, 2004.

5 Kikegawa, Y., Genchi, Y., Yoshikado, H., and Kondo, H.: Development of a numerical simulation system toward comprehensive assessments of urban warming countermeasures including their impacts upon the urban buildings' energy-demands, Appl. Energ., 76, 449–466, https://doi.org/10.1016/S0306-2619(03)00009-6, 2003.

Kleerekoper, L., van Esch, M., and Salcedo, T. B.: How to make a city climate-proof, addressing the urban heat island effect, Resour. Conserv. Recy., 64, 30–38, https://doi.org/10.1016/j.resconrec.2011.06.004, 2012.

10 Klein, P. and Clark, J. V.: Flow variability in a North American downtown street canyon, J. Appl. Meteorol. Clim., 46, 851–877, 2007.

Klein, P. M. and Galvez, J. M.: Flow and turbulence characteristics in a suburban street canyon, Environ. Fluid Mech., 15, 419–438, 2015.

Kochanski, A. K., Pardyjak, E. R., Stoll, R., Gowardhan, A., Brown, M. J., and Steenburgh, W. J.: One-way coupling of the WRF-QUIC urban dispersion modeling system, J. Appl. Meteorol. Clim., 54, 2119–2139, https://doi.org/10.1175/JAMC-D-15-0020.1, 2015.

Kondo, H., Genchi, Y., Kikegawa, Y., Ohashi, Y., Yoshikado, H., and Komiyama, H.: Development of a multi-layer urban canopy model for

15 the analysis of energy consumption in a big city: structure of the urban canopy model and its basic performance, Bound.-Lay. Meteorol., 116, 395–421, https://doi.org/10.1007/s10546-005-0905-5, 2005.

Kono, T., Ashie, Y., and Tamura, T.: Mathematical derivation of spatially-averaged momentum equations for an urban canopy model using underlying concepts of the immersed boundary method, Bound.-Lay. Meteorol., 135, 185–207, https://doi.org/10.1007/s10546-010-9475-2, 2010.

20 Krayenhoff, E., Christen, A., Martilli, A., and Oke, T.: A multi-layer radiation model for urban neighbourhoods with trees, Bound.-Lay. Meteorol., 151, 139–178, https://doi.org/10.1007/s10546-013-9883-1, 2014.

Krayenhoff, E. S.: A multi-layer urban canopy model for neighbourhoods with trees, Ph.D. thesis, University of British Columbia, https://doi.org/10.14288/1.0167084, 2014.

Krayenhoff, E. S. and Voogt, J. A.: A microscale three-dimensional urban energy balance model for studying surface temperatures, Bound.-

25 Lay. Meteorol., 123, 433–461, https://doi.org/10.1007/s10546-006-9153-6, 2007.

Krayenhoff, E. S., Santiago, J.-L., Martilli, A., Christen, A., and Oke, T. R.: Parametrization of drag and turbulence for urban neighbourhoods with trees, Bound.-Lay. Meteorol., 156, 157–189, https://doi.org/10.1007/s10546-015-0028-6, 2015.

Krayenhoff, E. S., Jiang, T., Christen, A., Martilli, A., Oke, T. R., Bailey, B. N., Nazarian, N., Voogt, J. A., Giometto, M. G., Stastny, A., et al.: A multi-layer urban canopy meteorological model with trees (BEP-Tree): Street tree impacts on pedestrian-level climate, Urban

30 Climate, 32, 100 590, https://doi.org/10.1016/j.uclim.2020.100590, 2020.

Kusaka, H., Kondo, H., Kikegawa, Y., and Kimura, F.: A simple single-layer urban canopy model for atmospheric models: comparison with multi-layer and slab models, Bound.-Lay. Meteorol., 101, 329–358, https://doi.org/10.1023/A:1019207923078, 2001.

Lauwaet, D., De Ridder, K., Saeed, S., Brisson, E., Chatterjee, F., van Lipzig, N., Maiheu, B., and Hooyberghs, H.: Assessing the current and future urban heat island of Brussels, Urban Climate, 15, 1 – 15, https://doi.org/10.1016/j.uclim.2015.11.008, 2016.

35 Lee, S.-H. and Park, S.-U.: A vegetated urban canopy model for meteorological and environmental modelling, Bound.-Lay. Meteorol., 126, 73–102, https://doi.org/10.1007/s10546-007-9221-6, 2008.

Lemonsu, A., Masson, V., Shashua-Bar, L., Erell, E., and Pearlmutter, D.: Inclusion of vegetation in the Town Energy Balance model for modelling urban green areas, Geosci. Model Dev., 5, 1377–1393, https://doi.org/10.5194/gmd-5-1377-2012, 2012.

Louis, J.-F.: A parametric model of vertical eddy fluxes in the atmosphere, Bound.-Lay. Meteorol., 17, 187–202, https://doi.org/10.1007/BF00117978, 1979.

Lundquist, K. A., Chow, F. K., and Lundquist, J. K.: An immersed boundary method for the weather research and forecasting model, Mon. Weather Rev., 138, 796–817, https://doi.org/10.1175/2009MWR2990.1, 2010.

5   Maronga, B., Gryschka, M., Heinze, R., Hoffmann, F., Kanani-Sühring, F., Keck, M., Ketelsen, K., Letzel, M. O., Sühring, M., and Raasch, S.: The Parallelized Large-Eddy Simulation Model (PALM) version 4.0 for atmospheric and oceanic flows: model formulation, recent developments, and future perspectives, Geosci. Model Dev., 8, 2515–2551, https://doi.org/10.5194/gmd-8-2515-2015, 2015.

Martilli, A. and Santiago, J. L.: CFD simulation of airflow over a regular array of cubes. Part II: analysis of spatial average properties, Bound.-Lay. Meteorol., 122, 635–654, https://doi.org/10.1007/s10546-006-9124-y, 2007.

10   Martilli, A., Clappier, A., and Rotach, M. W.: An urban surface exchange parameterisation for mesoscale models, Bound.-Lay. Meteorol., 104, 261–304, https://doi.org/10.1023/A:1016099921195, 2002.

Masson, V.: A physically-based scheme for the urban energy budget in atmospheric models, Bound.-Lay. Meteorol., 94, 357–397, https://doi.org/10.1023/A:1002463829265, 2000.

Masson, V., Grimmond, C. S. B., and Oke, T. R.: Evaluation of the Town Energy Balance (TEB) scheme with direct measurements from dry
15   districts in two cities, J. Appl. Meteorol., 41, 1011–1026, https://doi.org/10.1175/1520-0450(2002)041<1011:EOTTEB>2.0.CO;2, 2002.

Masson, V., Gomes, L., Pigeon, G., Liousse, C., Pont, V., Lagouarde, J. P., Voogt, J., Salmond, J., Oke, T. R., Hidalgo, J., Legain, D., Garrouste, O., Lac, C., Connan, O., Briottet, X., Lachérade, S., and Tulet, P.: The Canopy and Aerosol Particles Interactions in TOlouse Urban Layer (CAPITOUL) experiment, Meterol. Atmos. Phys., 102, 135–157, https://doi.org/10.1007/s00703-008-0289-4, 2008.

Mauree, D., Blond, N., and Clappier, A.: Multi-scale modeling of the urban meteorology: Integration of a new canopy model in the WRF
20   model, Urban Climate, 26, 60–75, https://doi.org/10.1016/j.uclim.2018.08.002, 2018.

Meili, N., Manoli, G., Burlando, P., Bou-Zeid, E., Chow, W. T. L., Coutts, A. M., Daly, E., Nice, K. A., Roth, M., Tapper, N. J., Velasco, E., Vivoni, E. R., and Fatichi, S.: An urban ecohydrological model to quantify the effect of vegetation on urban climate and hydrology (UT&C v1.0), Geosci. Model Dev., 13, 335–362, https://doi.org/10.5194/gmd-13-335-2020, 2020.

Mills, G.: An urban canopy-layer climate model, Theor. Appl. Climatol., 57, 229–244, https://doi.org/10.1007/BF00863615, 1997.

25   Moeng, C.-H., Dudhia, J., Klemp, J., and Sullivan, P.: Examining two-way grid nesting for large eddy simulation of the PBL using the WRF model, Mon. Weather Rev., 135, 2295–2311, https://doi.org/10.1175/MWR3406.1, 2007.

Monin, A. S. and Obukhov, A. M.: Basic regularity in turbulent mixing in the surface layer of the atmosphere, Tr. Akad. Nauk SSSR Geophiz. Inst., 1957.

Mussetti, G., Brunner, D., Henne, S., Allegrini, J., Krayenhoff, E. S., Schubert, S., Feigenwinter, C., Vogt, R., Wicki, A., and Carmeliet, J.:
30   COSMO-BEP-Tree v1.0: a coupled urban climate model with explicit representation of street trees, Geosci. Model Dev., 13, 1685–1710, https://doi.org/10.5194/gmd-13-1685-2020, 2020.

Nazarian, N. and Kleissl, J.: Realistic solar heating in urban areas: air exchange and street-canyon ventilation, Build. Environ., 95, 75–93, https://doi.org/10.1016/j.buildenv.2015.08.021, 2016.

Nazarian, N., Martilli, A., and Kleissl, J.: Impacts of realistic urban heating, Part I: spatial variability of mean flow, turbulent exchange and
35   pollutant dispersion, Bound.-Lay. Meteorol., 166, 367–393, https://doi.org/10.1007/s10546-017-0311-9, 2018.

Nazarian, N., Krayenhoff, E. S., and Martilli, A.: A one-dimensional model of turbulent flow through "urban" canopies (MLUCM v2.0): updates based on large-eddy simulation, Geosci. Model Dev., 13, 937–953, https://doi.org/10.5194/gmd-13-937-2020, 2020.

Paulson, C. A.: The mathematical representation of wind speed and temperature profiles in the unstable atmospheric surface layer, J. Appl. Meteorol., 9, 857–861, https://doi.org/10.1175/1520-0450(1970)009<0857:TMROWS>2.0.CO;2, 1970.

Pope, S. B.: Turbulent flows, Cambridge University Press, Cambridge, https://doi.org/10.1017/CBO9780511840531, 2000.

Raupach, M. R., Antonia, R. A., and Rajagopalan, S.: Rough-Wall Turbulent Boundary Layers, Appl. Mech. Rev., 44, 1–25, 1991.

5   Redon, E. C., Lemonsu, A., Masson, V., Morille, B., and Musy, M.: Implementation of street trees within the solar radiative exchange parameterization of TEB in SURFEX v8.0, Geosci. Model Dev., 10, 385–411, https://doi.org/10.5194/gmd-10-385-2017, 2017.

Resler, J., Krč, P., Belda, M., Juruš, P., Benešová, N., Lopata, J., Vlček, O., Damašková, D., Eben, K., Derbek, P., Maronga, B., and Kanani-Sühring, F.: PALM-USM v1. 0: A new urban surface model integrated into the PALM large-eddy simulation model, Geosci. Model Dev., 10, 3635–3659, https://doi.org/10.5194/gmd-10-3635-2017, 2017.

10   Rotach, M. W., Vogt, R., Bernhofer, C., Batchvarova, E., Christen, A., Clappier, A., Feddersen, B., Gryning, S. E., Martucci, G., Mayer, H., Mitev, V., Oke, T. R., Parlow, E., Richner, H., Roth, M., Roulet, Y. A., Ruffieux, D., Salmond, J. A., Schatzmann, M., and Voogt, J. A.: BUBBLE–an Urban boundary layer meteorology project, Theor. Appl. Climatol., 81, 231–261, https://doi.org/10.1007/s00704-004-0117-9, 2005.

Roth, M.: Review of atmospheric turbulence over cities, Q. J. R. Meteorol. Soc., 126, 941–990, https://doi.org/10.1002/qj.49712656409, 15   2000.

Runnalls, K. E. and Oke, T. R.: Dynamics and controls of the near-surface heat island of Vancouver, British Columbia, Physical Geography, 21, 283–304, https://doi.org/10.1080/02723646.2000.10642711, 2000.

Ryu, Y.-H., Baik, J.-J., and Lee, S.-H.: A new single-layer urban canopy model for use in mesoscale atmospheric models, J. Appl. Meteorol. Clim., 50, 1773–1794, https://doi.org/10.1175/2011JAMC2665.1, 2011.

20   Ryu, Y.-H., Bou-Zeid, E., Wang, Z.-H., and Smith, J. A.: Realistic representation of trees in an urban canopy model, Bound.-Lay. Meteorol., 159, 193–220, https://doi.org/10.1007/s10546-015-0120-y, 2016.

Salamanca, F., Krpo, A., Martilli, A., and Clappier, A.: A new building energy model coupled with an urban canopy parameterization for urban climate simulations—part I. formulation, verification, and sensitivity analysis of the model, Theor. Appl. Climatol., 99, 331–344, https://doi.org/10.1007/s00704-009-0142-9, 2010.

25   Salamanca, F., Georgescu, M., Mahalov, A., Moustaoui, M., and Wang, M.: Anthropogenic heating of the urban environment due to air conditioning, J. Geophys. Res.-Atmos., 119, 5949–5965, https://doi.org/10.1002/2013JD021225, 2014.

Saneinejad, S., Moonen, P., Defraeye, T., Derome, D., and Carmeliet, J.: Coupled CFD, radiation and porous media transport model for evaluating evaporative cooling in an urban environment, J. Wind. Eng. Ind. Aerodyn., 104-106, 455–463, https://doi.org/10.1016/j.jweia.2012.02.006, 2012.

30   Santiago, J. L. and Martilli, A.: A dynamic urban canopy parameterization for mesoscale models based on computational fluid dynamics Reynolds-Averaged Navier-Stokes microscale simulations, Bound.-Lay. Meteorol., 137, 417–439, https://doi.org/10.1007/s10546-010-9538-4, 2010.

Simón-Moral, A., Santiago, J. L., and Martilli, A.: Effects of unstable thermal stratification on vertical fluxes of heat and momentum in urban areas, Bound.-Lay. Meteorol., 163, 103–121, https://doi.org/10.1007/s10546-016-0211-4, 2017.

35   Soulhac, L., Salizzoni, P., Cierco, F.-X., and Perkins, R.: The model SIRANE for atmospheric urban pollutant dispersion; part I, presentation of the model, Atmos. Environ., 45, 7379–7395, https://doi.org/10.1016/j.atmosenv.2011.07.008, 2011.

Stull, R. B.: An introduction to boundary layer meteorology, Kluwer Academic Publishers, Dordrecht, The Netherlands, https://doi.org/10.1007/978-94-009-3027-8, 1988.

Talbot, C., Bou-Zeid, E., and Smith, J.: Nested mesoscale large-eddy simulations with WRF: performance in real test cases, J. Hydrometeorol., 13, 1421–1441, https://doi.org/10.1175/JHM-D-11-048.1, 2012.

Tseng, Y.-H., Meneveau, C., and Parlange, M. B.: Modeling flow around bluff bodies and predicting urban dispersion using large eddy simulation, Environ. Sci. Technol., 40, 2653–2662, https://doi.org/10.1021/es051708m, 2006.

5   Wang, C., Wang, Z.-H., and Yang, J.: Cooling effect of urban trees on the built environment of contiguous United States, Earth's Future, 6, 1066–1081, https://doi.org/10.1029/2018EF000891, 2018.

Wang, H., Skamarock, W. C., and Feingold, G.: Evaluation of scalar advection schemes in the advanced research WRF model using large-eddy simulations of aerosol-cloud interactions, Mon. Weather Rev., 137, 2547–2558, https://doi.org/10.1175/2009MWR2820.1, 2009.

Wang, Z.-H.: Geometric effect of radiative heat exchange in concave structure with application to heating of steel I-sections in fire, Int. J.
10   Heat Mass Tran., 53, 997–1003, https://doi.org/10.1016/j.ijheatmasstransfer.2009.11.013, 2010.

Wang, Z.-H.: Monte Carlo simulations of radiative heat exchange in a street canyon with trees, Sol. Energy, 110, 704 – 713, https://doi.org/10.1016/j.solener.2014.10.012, 2014.

Wang, Z.-H., Bou-Zeid, E., and Smith, J. A.: A coupled energy transport and hydrological model for urban canopies evaluated using a wireless sensor network, Q. J. Roy. Meteor. Soc., 139, 1643–1657, https://doi.org/10.1002/qj.2032, 2013.

15   Yaghoobian, N. and Kleissl, J.: Effect of reflective pavements on building energy use, Urban Climate, 2, 25–42, https://doi.org/10.1016/j.uclim.2012.09.002, 2012.

Yang, H., abd Mary Heskel, X. Y., Sun, S., and Tang, J.: Seasonal variations of leaf and canopy properties tracked by ground-based NDVI imagery in a temperate forest, Sci. Rep.-UK, 7, 1267, https://doi.org/10.1038/s41598-017-01260-y, 2017.

Yang, X. and Li, Y.: The impact of building density and building height heterogeneity on average urban albedo and street surface temperature,
20   Build. Environ., 90, 146–156, https://doi.org/10.1016/j.buildenv.2015.03.037, 2015.

Zajic, D., Fernando, H. J. S., Calhoun, R., Princevac, M., Brown, M. J., and Pardyjak, E. R.: Flow and turbulence in an urban canyon, J. Appl. Meteorol. Clim., 50, 203–223, https://doi.org/10.1175/2010JAMC2525.1, 2011.

Zeng, X. and Dickinson, R. E.: Effect of surface sublayer on surface skin temperature and fluxes, J. Climate, 11, 537–550, https://doi.org/10.1175/1520-0442(1998)011<0537:EOSSOS>2.0.CO;2, 1998.